Cellular/Molecular

Altered Electrophysiology and Transcriptome of GnRH Neurons in Middle-Aged Female Mice

Imre Farkas,[1,2*] Csaba Vastagh,[1,3*] Imre Kalló,[1] Levente Kontra,[4] and Zsolt Liposits[1]

[1]Laboratory of Endocrine Neurobiology, [2]Laboratory of Reproductive Neurobiology, [3]Laboratory of Integrative Neuroendocrinology, and [4]Bioinformatics Core Facility, HUN-REN Institute of Experimental Medicine, Budapest H-1083, Hungary

Aging affects the reproductive system, although its impact on GnRH neurons is mainly unexplored. Thus, we compared the transcriptome and electrophysiology of GnRH neurons obtained from female middle-aged (MA, 400–430 d) and young (Y, 70 d), diestrous mice, respectively. Transcriptomic analysis revealed reproductive senescence-related molecular changes in one-third of the MA mice. The upregulated genes ($n = 225$) were linked to immune signaling, olfactory- and vomeronasal receptors. The downregulated genes ($n = 233$) were related to mRNA processing, G-protein–coupled receptors, oxidative phosphorylation, electron transport, and estrogen signaling. In addition, ion channel (Na, K, Ca), neurotransmitter (ACh, GABA, glutamate), and various neuropeptide receptor-coding genes showed differential expression indicating functional alterations of the cells. Accordingly, whole-cell patch–clamp recordings revealed a twofold increase in spontaneous firing frequency of MA-GnRH neurons. Significant changes were also observed in characteristics of action potentials and afterhyperpolarization amplitudes. Conspicuously, miniature postsynaptic currents were absent in 72% of MA-GnRH neurons, and pharmacological blockade of $GABA_A$ and glutamate receptors didn't affect the firing rate. However, administration of their ligands evoked inward currents and facilitated firing in both animal groups, although with a decreased efficacy in MA animals. MA-GnRH neurons sustained responsiveness to estradiol, G-protein inhibition, and kisspeptin (KP) like those of young animals. While KP receptor antagonist, KP-234, diminished firing frequency of MA-GnRH neurons, it had no effect on young GnRH cells. Collectively, these findings revealed that both the transcriptome and electrophysiological activity of GnRH neurons change at middle age and the explored alterations are hallmarks of early phase of reproductive senescence.

Key words: aging; electrophysiology; female; GnRH; mouse; transcriptome

Significance Statement

Aging reduces gonadal hormone production, which is centrally regulated by GnRH neurons. Understanding how the early phase of reproductive senescence affects the GnRH system is crucial. Using middle-aged (MA) female mice, we demonstrate that GnRH neurons undergo transcriptomic changes indicating altered, house-keeping mechanisms and modification of cellular activity. Accordingly, MA-GnRH neurons showed increased firing activity despite the attenuated GABA and glutamate neurotransmission and sustained estradiol responsiveness. G-protein–coupled receptor signaling remained functional, and kisspeptin (KP) further increased the firing frequency. Contrasting young GnRH neurons, the MA cells received a tonic KP modulation. These findings also highlight the heterogeneity of MA mice population and provide molecular and functional markers of GnRH neurons characteristic for the early phase of reproductive senescence.

Introduction

Gonadotropin-releasing hormone (GnRH; Matsuo et al., 1971) is synthesized by a distinct neuron population in the rodent forebrain (Silverman et al., 1979; Merchenthaler et al., 1980; Liposits et al., 1984; Wetsel et al., 1992; Campbell et al., 2005, 2022). It plays a significant role in regulating reproduction via the hypothalamic–pituitary–gonadal (HPG) axis (Knobil, 1988). Disruptions in differentiation and migration of GnRH

Received Feb. 26, 2025; revised Sept. 20, 2025; accepted Sept. 23, 2025.

Author contributions: I.F., C.V., and Z.L. designed research; I.F., C.V., and I.K. performed research; I.F., C.V., I.K., and L.K. analyzed data; I.F., C.V., I.K., and Z.L. wrote the paper.

We express our gratitude to Dr. Suzanne M. Moenter (Department of Molecular and Integrative Physiology, University of Michigan) for the kind donation of the GnRH-GFP transgenic mice used in this study. We thank Dr. Richárd Sinkó (Molecular Cell Metabolism Research Group, HUN-REN Institute of Experimental Medicine) for his advice in the statistical analyses. Project no. RRF-2.3.1-21-2022-00011, titled National Laboratory of Translational Neuroscience, has been implemented with the support provided by the Recovery and Resilience Facility of the European Union within the framework of Programme Széchenyi Plan Plus. This work was supported by National Research, Development and Innovation Office K142357 and Programme Széchenyi Plan Plus, RRF-2.3.1-21-2022-00011, to Z.L. The funder had no role in the design of the study, data collection and interpretation, or the decision to submit the work for publication.

*I.F. and C.V. contributed equally to this work.

The authors declare no competing financial interests.

Correspondence should be addressed to Imre Farkas at farkas.imre@koki.hu or Zsolt Liposits at liposits.zsolt@koki.hu.

https://doi.org/10.1523/JNEUROSCI.0410-25.2025

neurons (Wray et al., 1989) or impairments of their regulatory networks lead to reproductive failure, ranging from severe dysfunction to infertility (Pitteloud et al., 2006, 2007). Beyond reproduction, diminished levels of gonadal hormones impact multiple organ systems (Korach, 1994; Imamov et al., 2005).

In females, the HPG axis undergoes cyclic changes throughout reproductive period, followed by perimenopause leading to reproductive senescence and, ultimately, menopause (Gore et al., 2000; Brinton et al., 2015). Perimenopause is characterized by declining fertility and altering hormonal levels and requires special attention in humans due to its association with somatic disturbances and mood disorders (Parry, 2008; Santoro et al., 2021).

Middle-aged (MA) rodents serve as a well-established experimental model for studying the early biological events of reproductive senescence (Kermath and Gore, 2012). In mice, individuals aged 10–15 months are classified as MA (Flurkey et al., 2007). During this phase, ovarian cycles become irregular and may extend to 6 d, although both regularly cycling and acyclic individuals exist within the population (Nelson et al., 1981, 1982). Serum estradiol levels decline progressively with age (Nelson et al., 1981, 1992; Yan et al., 2017), reflecting the heterogeneous nature of ovarian function in MA mice. By 25 months, all mice become acyclic (Frick et al., 2000).

Reproductive aging also alters hypothalamic function. In MA rodents, the luteinizing hormone surge is blunted and delayed (Wise et al., 1988; Scarbrough and Wise, 1990; Matt et al., 1998). This is accompanied by a decline in the proportion of GnRH neurons expressing c-Fos during the proestrous LH surge (Rubin et al., 1994) and the absence of the expected increase in GnRH primary transcript mRNA levels on the afternoon of the LH surge (Gore et al., 2000). These findings suggest that GnRH neurons play a key role in the process of reproductive senescence.

Interestingly, morphology of the GnRH neuronal network in MA mice remains largely unchanged from that of young animals (Hoffman and Finch, 1986). However, in terms of function, the pulsatile and surge-like release of GnRH (Czieselsky et al., 2016) undergoes significant modifications.

GnRH neurons can exhibit intrinsic pulsatility, as demonstrated in immortalized GnRH cell lines (Wetsel et al., 1992) and in primary neurons derived from nasal explants (Constantin et al., 2009). The activity of GnRH neurons is modulated by major neurotransmitters, including GABA (DeFazio et al., 2002; Iremonger et al., 2010), glutamate (Iremonger et al., 2010), and acetylcholine (Shostak et al., 2023; Vastagh et al., 2024), as well as various neuropeptides (Spergel, 2019). Among these neuromodulators, kisspeptin (KP) plays a crucial role in controlling both pulsatile and surge-like GnRH release (Han et al., 2005; Clarke et al., 2015; Xie et al., 2022).

In addition to synaptic inputs, GnRH neurons are subject to hormonal regulation. Estradiol exerts both positive and negative feedback effects on GnRH neurons, fine-tuning reproductive function (Moenter et al., 2009, 2020). These effects are mediated not only directly on GnRH neurons (Bálint et al., 2016; Farkas et al., 2018) but also via kisspeptinergic neurons, which are highly sensitive to estradiol (Pielecka-Fortuna et al., 2008; Rønnekleiv et al., 2015; Wang et al., 2016).

Since the discovery of GnRH, most studies have focused on molecular, anatomical, and functional properties of the system in young animals. Nonetheless, how aging affects GnRH neurons at the cellular and transcriptome levels is poorly understood. Given the crucial role of GnRH neurons in the control of reproduction, investigating their molecular and functional adaptations during middle age is essential for understanding the mechanisms of early phase of reproductive senescence.

Materials and Methods

Animals

Expression profiling. Adult female GnRH-GFP transgenic mice (Suter et al., 2000) were obtained from local colonies bred at the Medical Gene Technology Unit of the Institute of Experimental Medicine (IEM). All animals were housed in a controlled environment with a 12:12 h light/dark cycle (lights on at 06:00 A.M.), ambient temperature of 22 ± 2°C, and *ad libitum* access to standard food and water. Experimental groups are follows: young (Y, 70–90 d; $N = 8$) and MA (400–430 d; $N = 8$). The estrous cycle was monitored via microscopic evaluation of the vaginal smears, collected daily between 9:00 and 11:00 A.M., prior to termination at the diestrous phase. Diestrus was identified by a predominance of leukocytes in vaginal smears and uterine mass below 100 mg.

The phenotype of the reproductive system of MA female mice has previously been reported to show only minor alterations compared with young controls including changes in the estrous cycle with a longer diestrous phase and a slightly increased uterine weight (Flurkey et al., 2007; Balough et al., 2024), as well as a tendency toward higher basal LH levels (Parkening et al., 1982). The reproductive phenotype of the MA mice used in our laboratory is in line with these published hallmarks.

Surgical interventions and perfusions were performed under deep anesthesia, induced via intraperitoneal injection of ketamine (25 mg/kg) and xylazine (5 mg/kg). GFP expression was observed in 84–94% of GnRH-immunopositive neurons (Vastagh et al., 2024).

Electrophysiology. Acute hypothalamic slices were prepared from young, diestrous ($N = 28$) and MA ($N = 52$) female GnRH-GFP mice under deep anesthesia, as written above. The animals were transcardially perfused with ice-cold sucrose–containing cutting solution (~50 ml) containing (in mM) 218.3 sucrose, 2 KCl, 25 $NaHCO_3$, 1.2 NaH_2PO_4, 1 $CaCl_2$, 1 $MgSO_4$, 0.01 glycine, and 10 D-glucose, saturated with carbogen gas (95% O_2/5% CO_2). The brains were then removed following decapitation and further chilled in ice-cold sucrose–containing cutting solution for 2 min.

Ethics statement

All animal studies were conducted with the approval of the Animal Welfare Committee of the Institute of Experimental Medicine (Permission Number: PE/EA/00646-6/2022) and in compliance with the legal requirements of the European Community (Directive 2010/63/EU). All experiments adhered to internationally accepted standards for humane animal care, with every effort made to minimize animal suffering.

Experimental design and statistical analysis

Gene expression profiling. Microarray analysis was conducted to identify potential age-related changes in gene expression and signaling pathways in GnRH neurons from young [postnatal day (P)70–90] and MA, diestrous (P400–430) female mice. The diestrous stage was chosen to reduce variability and improve the reliability of microarray data analysis.

To standardize experimental conditions, animals from both age groups were housed in the same facility under identical environmental conditions. They were perfused at the diestrous stage with 0.5% paraformaldehyde to preserve mRNA integrity and GFP signal in GnRH neurons. The tissue and RNA sample preparation were fully randomized to eliminate batch effects.

Thin, frozen brain sections containing GnRH neurons were obtained, and individual GFP-expressing GnRH neurons were microdissected in a uniform random manner to ensure unbiased sampling of the entire neuronal population. GnRH neurons were pooled by the brain, followed by total RNA isolation and whole transcriptome amplification (WTA). The WTA method allowed for effective amplification of low-quantity RNA from the formalin-fixed tissue without introducing 3′ bias. Equal amounts of cDNA were used for fragmentation and labeling before microarray hybridization.

To ensure data quality, a preprocessing pipeline was applied to the raw microarray dataset, including background correction and normalization, followed by principal component analysis (PCA) to identify

clustering patterns and potential outliers. Differential gene expression analysis between age groups was performed using linear models (limma) to ensure unbiased estimation of gene expression differences. Fold change (FC) values were calculated as the ratio of expression levels between the two groups. To improve reliability, particularly given the limited sample size, empirical Bayes methods were employed to stabilize variance estimates. Moderated *t* tests were used to compare gene expression levels between groups. Multiple hypothesis testing was controlled using the Benjamini–Hochberg (BH) procedure, with a false discovery rate (FDR) threshold of 0.05 applied for differential gene expression analysis.

Pathway enrichment analysis was performed using overrepresentation analysis (ORA) and gene set enrichment analysis (GSEA). ORA was used to assess the significant enrichment of differentially expressed genes (DEGs) relative to a background gene set. For ORA, Fisher's exact test was applied to Gene Ontology (GO) pathways. GSEA was conducted using a functional class scoring approach to identify overrepresented or underrepresented gene classes. WikiPathways was selected as the primary database for its community-driven updates, high granularity, and open-access integration. GSEA results were filtered using Kolmogorov–Smirnov statistics.

Whole-cell patch–clamp studies. Firing activity, membrane currents, and miniature postsynaptic currents (mPSCs) were recorded using current- and voltage-clamp techniques in GnRH neurons from acute brain slices of GnRH-GFP mice. First, various parameters of action potentials (APs) and spontaneous firing activity were compared between young and MA mice. Current-clamp recordings were used to assess differences in spontaneous firing rates. The homogeneity or heterogeneity of firing rate data was analyzed using cluster analysis. Positive and negative square current pulses were applied to evaluate the evoked firing rate, AP amplitude, AP duration at half-amplitude, and afterhyperpolarization (AHP). Negative pulses were used to assess passive parameters such as input resistance and capacitance.

Second, the integrity of the afferent neurotransmitter systems controlling GnRH neurons was examined. mPSCs were recorded using voltage-clamp techniques in the presence of sequentially applied various neurotransmitter receptor blockers. Then, effects of extracellularly applied GABA and glutamate, administered in a single bolus onto the slice, were assessed by measuring changes in the firing rate or membrane current. Additionally, firing activity was analyzed in the presence of neurotransmitter blockers.

Third, the responsiveness of GnRH neurons to 17β-estradiol (E2) was assessed by measuring changes in spontaneous firing rates using current-clamp recordings. Low (10 pM) and high (200 pM) doses of E2 were applied as single boluses onto the slice during electrophysiological recordings.

Fourth, the roles of the GnRH and KP in modulating the firing characteristics of GnRH neurons in MA mice were investigated. Spontaneous firing activity was recorded in the presence of the membrane-impermeable G-protein inhibitor GDP-β-S, the GnRH receptor (GnRH-R) antagonist Antide, and the KP receptor (KP-R) antagonist KP-234 using current-clamp techniques. Additionally, the effect of KP, applied in a single bolus, on the firing rate was examined.

Cluster analysis with the Mann–Whitney test was used to assess potential heterogeneity in the firing rate data of GnRH neurons from MA mice. Due to observed heterogeneity, nonparametric tests were employed: the Wilcoxon test was used for paired firing rate data, while the Friedman test was applied to sequential multiple firing rate measurements. Repeated-measures two-way ANOVA with Fisher's post hoc test was used to analyze effects of the various drugs on the firing rate of young versus MA animals. Student's *t* test was used to analyze evoked inward current data. Statistical analyses are presented in extended tables linked to the corresponding figures illustrating the results. Each neuron served as its own control for drug effect evaluations.

Gene expression profiling of MA-GnRH neurons

Sample preparation. Brain fixation and preparation of sections for laser capture microdissection (LCM) were conducted as previously described (Khodosevich et al., 2007; Vastagh et al., 2015). Briefly, young ($n = 8$) and MA ($n = 8$) diestrous female GnRH-GFP transgenic mice were deeply anesthetized and perfused transcardially with 80 ml of 0.5% paraformaldehyde, followed by 50 ml of 20% sucrose in PBS. For LCM, 8-µm-thick coronal brain sections were cut, mounted on PEN-membrane slides (MembraneSlide 1.0 PEN, Carl Zeiss Microimaging), air-dried, and sequentially treated with 50% ethanol (20 s), *n*-butanol/ethanol (25:1, 90 s), and xylene substitution/*n*-butanol (25:1, 60 s). The slides were stored at −80°C in air-tight containers containing silica gel desiccant.

For transcriptome profiling GnRH-GFP neurons were dissected from their entire rostrocaudal path, stretching from the medial septum via the vertical limb of the diagonal band of Broca down to the medial preoptic area (MPOA). Laser-microdissected GnRH neurons were pressure-catapulted into 0.5 ml tube caps (Adhesive Cap 500, Carl Zeiss) at 40× magnification using a PALM MicroBeam system (Carl Zeiss) equipped with an epifluorescent setup. A total of 303 ± 24 (mean ± SEM) dissected GFP-positive cell profiles were pooled from 80 to 100 consecutive sections per brain.

RNA was extracted using the Arcturus Paradise Plus RNA Extraction and Isolation Kit (Applied Biosystems). RNA integrity numbers were determined using an Agilent 2100 Bioanalyzer (Agilent) and ranged between 5.5 and 7.6 for the test sections.

Microarray analysis. Total RNA was reverse transcribed and amplified using the WTA method (WTA2, Sigma-Aldrich). Amplification was monitored via SYBR Green on a CFX96 real-time PCR system (Bio-Rad Laboratories) and stopped at 28 cycles, once fluorescence plateaued. The cDNA was purified using the PureLink Quick PCR Purification Kit (Invitrogen) and quantified with a Nanodrop One microvolume spectrophotometer (Thermo Fisher Scientific). Eight micrograms of cDNA were fragmented and labeled using the GeneChip Mapping 250 K Nsp Assay Kit (Affymetrix) according to the manufacturer's instructions.

Array hybridization was performed using the GeneChip Hybridization, Wash, and Stain Kit (Applied Biosystems). Libraries were denatured at 99° C for 2 min and then incubated on the Clariom S Mouse Assay array (Applied Biosystems). Hybridization lasted 16 h at 45°C and 60 rpm in the GeneChip Hybridization Oven 645 (Affymetrix/Thermo Fisher Scientific). Washing and staining were performed using the GeneChip Fluidics Station 450, following the Clariom S Mouse Array protocol (Affymetrix/Thermo Fisher Scientific). Arrays were then scanned with the GeneChip Scanner GCS3000 (Affymetrix/Thermo Fisher Scientific) under default settings.

Raw CEL files were generated using the Command Console software (Affymetrix/Thermo Fisher Scientific) and were preprocessed by correcting for GC content, intensity scaling, and quality control checks via Analysis Power Tools (ver. 2.11.8, Thermo Fisher Scientific) before further bioinformatics analysis.

Bioinformatics. All statistical and data mining analyses were conducted in the R programming environment using packages from the Bioconductor project. Microarray quality assessment ($n = 16$) was performed using the arrayQualityMetrics R package (Kauffmann et al., 2009). Raw microarray data were preprocessed using the Robust Multichip Average (RMA) method for background correction and normalization, generating an expression matrix (Irizarry et al., 2003). PCA was conducted and visualized using a custom R function (Klaus and Reisenauer, 2016).

Differential gene expression was analyzed using linear models and empirical Bayesian statistics, implemented via the limma package (Ritchie et al., 2015). FC was computed from the normalized, log2-transformed gene expression matrix. Raw *p* values were adjusted using the BH method. DEGs were identified based on criteria of $FC > |2|$ and adjusted $p < 0.05$. The EnhancedVolcano R package (Blighe et al., 2024) was used to visualize differential gene expression between MA and young GnRH neurons. The top 50 DEGs were plotted using the ComplexHeatmap R package (Gu et al., 2016).

For ORA, a one-sided Fisher's exact test was employed to assess the significance of enrichment in GO pathways. Pathways were considered significantly enriched if the *q* values were <0.05, following multiple testing correction using the BH method.

GSEA (Subramanian et al., 2005) was conducted by ranking genes as the product of the sign of the log FC and the negative logarithm (base 10) of the *p* value that represents the statistical significance of the differential expression of each gene. The gseWP function from clusterProfiler (Xu et al., 2024) was used for pathway enrichment in WikiPathways (Agrawal et al., 2024), with a minimum gene set size of 10 and a maximum of 500. Pathway gene sets were considered significant when *q* values were <0.05. Pathway visualizations were generated in Cytoscape v3.10.0 (Shannon et al., 2003) via the RCy3 package (Gustavsen et al., 2019).

Electrophysiology

Slice electrophysiology. A Leica VT-1000S vibratome (Leica Microsystems) was used in a chilled metal chamber containing sucrose-containing cutting solution to obtain 220 µm coronal slices through the caudal part of the forebrain. For electrophysiological measurements, GnRH-GFP neurons residing in the vicinity of the OVLT were selected. The sampling territory included the median preoptic nucleus, the MPOA, the ventromedial preoptic nucleus, and the rostral tip of the anteroventral periventricular nucleus. The slices were immediately transferred to a holding chamber containing intermediate artificial cerebrospinal fluid (iaCSF) heated at 33°C (in mM: 124 NaCl, 2.5 KCl, 25 $NaHCO_3$, 1.23 NaH_2PO_4, 1 $CaCl_2$, 3 $MgSO_4$, and 10 D-glucose, saturated with 95% O_2/5% CO_2). The slices were allowed to equilibrate for at least 1 h in iaCSF before electrophysiological recordings started in normal aCSF (in mM: 126 NaCl, 3 KCl, 25 $NaHCO_3$, 1.2 NaH_2PO_4, 2.4 $CaCl_2$, 1.5 $MgSO_4$, and 11 D-glucose, saturated with 95% O_2/5% CO_2) in the measurement chamber.

Recordings were performed in carbogenated aCSF at 33°C using an Axopatch-200B patch-clamp amplifier, Digidata-1550B data acquisition system, and pCLAMP 10.7 software (Molecular Devices). Neurons were visualized using a BX51WI IR-DIC microscope (Olympus). Patch electrodes (OD, 1.5 mm; thin wall; Worcester Polytechnic Institute) were pulled with a Flaming-Brown P-97 puller (Sutter Instrument).

GnRH-GFP neurons were identified via brief illumination with a LED light source at 470 nm (CoolLED pE-100) through an epifluorescent filter set, based on their green fluorescence, typical fusiform shape, and characteristic topography (Suter et al., 2000).

Whole-cell patch–clamp recording. Spontaneous firing activity was recorded in a whole-cell current–clamp mode at 0 pA. Following a control period, agonists were applied as a single bolus directly onto the slice, and the firing recording was continued for an additional period (Table 1).

Table 1. Timing protocol for applying various agonists during recording of spontaneous firing

Agonist	Control period	Period after single bolus treatment	Total recording time
GABA or glutamate	5–10 s	70–75 s	80 s
10 pM or 200 pM E2	2 min	13 min	15 min
KP	1 min	5 min	6 min

For additional data, see Extended Data Figures 6-1–6-3, 7-1, and 8-1.

Extracellularly applied antagonist treatments (Antide, KP-234) began after a 1 min control period, and spontaneous firing activity was recorded for an additional 9 min, during which the inhibitors remained continuously present in the aCSF. For cumulative application of neurotransmitter blockers (picrotoxin, kynurenic acid, atropine, and mecamylamine), the blockers were sequentially added to the aCSF at different time points, picrotoxin at 1 min, kynurenic acid at 5 min, and atropine + mecamylamine at 10 min; the recording continued for up to 15 min.

For intracellularly applied GDP-β-S, the inhibitor was added to the pipette solution. Once the whole-cell configuration was achieved, spontaneous firing recordings commenced immediately and continued for 15 min.

Evoked firing and passive parameter measurements were conducted using 300 ms square current pulses (10 pulses), starting at 0 pA (pulse increments, +15 pA; first pulse is −60 pA). AP threshold was measured with a ramp of current injection (100 pA/2 s, starting from −60 pA).

Membrane current and mPSCs were recorded using the voltage-clamp mode at −70 mV holding potential. The intracellular pipette solution contained (in mM) 10 HEPES, 140 KCl, 5 EGTA, 0.1 $CaCl_2$, 4 Mg-ATP, 0.4 and Na-GTP), pH-adjusted to 7.3 with NaOH.

Patch electrodes had a resistance of 2–3 MΩ. Only cells with low holding current (<10 pA) and a stable baseline were used. Input resistance (R_{in}), series resistance (R_s), and membrane capacitance (C_m) were measured before and after each treatment using 5 mV hyperpolarizing pulses. To ensure consistent recording quality, only cells with R_s < 20 MΩ, R_{in} > 500 MΩ, and C_m > 10 pF were included in the analysis.

Spike-mediated transmitter release was blocked in all voltage-clamp experiments by adding the voltage-gated Na^+ channel inhibitor tetrodotoxin (TTX; 660 nM, Tocris Bioscience) to the aCSF 10 min before membrane current or mPSC recordings.

Evoked inward currents were triggered by GABA or glutamate following a 5–10 s control period, with recordings continuing for up to 80 s.

The mPSC recordings began with a 5 min control period, followed by sequential application of picrotoxin at 5 min and kynurenic acid at 10 min, with recordings continuing for an additional 15 min, while both blockers remained in the aCSF.

Chemicals used for electrophysiology. The chemicals used in the electrophysiological experiments are listed in Table 2 (Sung et al., 2000; Kuehl-Kovarik et al., 2002; Todman et al., 2005; Zhang et al., 2008; Yokoyama et al., 2014; Bálint et al., 2016; Farkas et al., 2016, 2018; Furuya et al., 2017; Vastagh et al., 2024).

Statistical analysis for electrophysiology. Recordings were stored and analyzed offline. Event detection was performed using the Clampfit module of the PClamp 10.7 software (Molecular Devices). Firing rates and mPSC frequencies were calculated as the number of APs or mPSCs divided by the corresponding time duration. The mean values of the control and treated periods were calculated from these frequency values. Group data were expressed as mean ± standard error of mean (SEM). Two-tailed Student's *t* test, Mann–Whitney *U* test, Wilcoxon test, Friedman test, two-way ANOVA with Fisher post hoc test, or comparative linear regression was used for group comparisons, with significance

Table 2. Chemicals used for electrophysiology

Chemical	Concentration	Supplier	Reference
TTX (Na^+-channel blocker)	660 nM	Tocris Bioscience (Number 1078)	Vastagh et al., 2024
Picrotoxin ($GABA_A$-R blocker)	100 µM	Tocris Bioscience (Number 1128)	Vastagh et al., 2024
Kynurenic acid (ionotropic glutamate-R blocker)	2 mM	Sigma-Aldrich (Number K3375)	Farkas et al., 2018
GABA	50 µM–1 mM	Tocris Bioscience (Number 0344)	Sung et al., 2000
L-Glutamic acid	1 mM	Tocris Bioscience (Number 0218)	Kuehl-Kovarik et al., 2002
Atropine (muscarinic ACh-R blocker)	10 µM	Sigma-Aldrich (Number A0132)	Furuya et al., 2017
Mecamylamine (nicotinic ACh-R blocker)	10 µM	Tocris Bioscience (Number 2843)	Furuya et al., 2017
Antide (GnRH-R antagonist)	100 nM	Bachem (Number 72)	Todman et al., 2005
GDP-β-S (G-protein inhibitor)	2 mM (intracellular)	Sigma-Aldrich (Number G7637)	Farkas et al., 2016
17β-Estradiol (E2)	10, 200 pM	Sigma-Aldrich (Number E2758)	Bálint et al., 2016; Farkas et al., 2018
KP-10	200 nM	Tocris Bioscience (Number 2570)	Zhang et al., 2008; Yokoyama et al., 2014
KP-234 (KP-R antagonist)	100 nM	Tocris Bioscience (Number 3881)	Yokoyama et al., 2014

For additional data, see Extended Data Figures 6-1–6-3, 7-1, and 8-1.

set at $p < 0.05$. The detailed statistical analysis results are presented in extended data tables linked to Figures 4–8.

Euclidean distance of firing rates was calculated for all MA samples to perform cluster analysis. Based on distance length, samples were clustered using the "complete" method from the hclust R package. Samples were subdivided at the first bifurcation to minimize intragroup distance. Mann–Whitney *U* test was applied to determine significant differences between putative subgroups. Additionally, the Mann–Whitney *U* test was used to compare differences between the MA subgroups and the young group.

Each neuron served as its own control for drug effect evaluations.

Results

Comparative gene expression profiling of young and MA-GnRH neurons

PCA reveals heterogeneity of MA mice

To investigate the impact of reproductive senescence on the transcriptome profile of GnRH neurons, GFP-positive neurons were microdissected for microarray analysis from young (Y) ($n = 8$) and MA ($n = 8$) diestrous GnRH-GFP mice. After data normalization, statistical comparisons of gene expression levels revealed significant differences. PCA showed that the MA group segregated into two distinct clusters (MA3 and MA5; Fig. 1*A*,*B*), prompting their consideration as separate subgroups. No DEGs (FDR < 0.05; FC > 2) were identified when comparing MA5 versus Y groups or when MA5 and MA3 were pooled together. Consequently, MA5 was excluded from further analysis. In contrast, when comparing MA3 versus Y, we identified 458 DEGs (233 downregulated, 225 upregulated; FDR < 0.05; FC > 2; Fig. 1*C*; Extended Data Figs. 1-1, 1-2), highlighting a distinct transcriptomic signature in MA3, which was used for subsequent pathway enrichment analysis. The boxplot representation of the top 50 DEGs is shown in Extended Data Figure 1-3. The statistics of the top 50 DEGs is disclosed in Extended Data Figure 1-4.

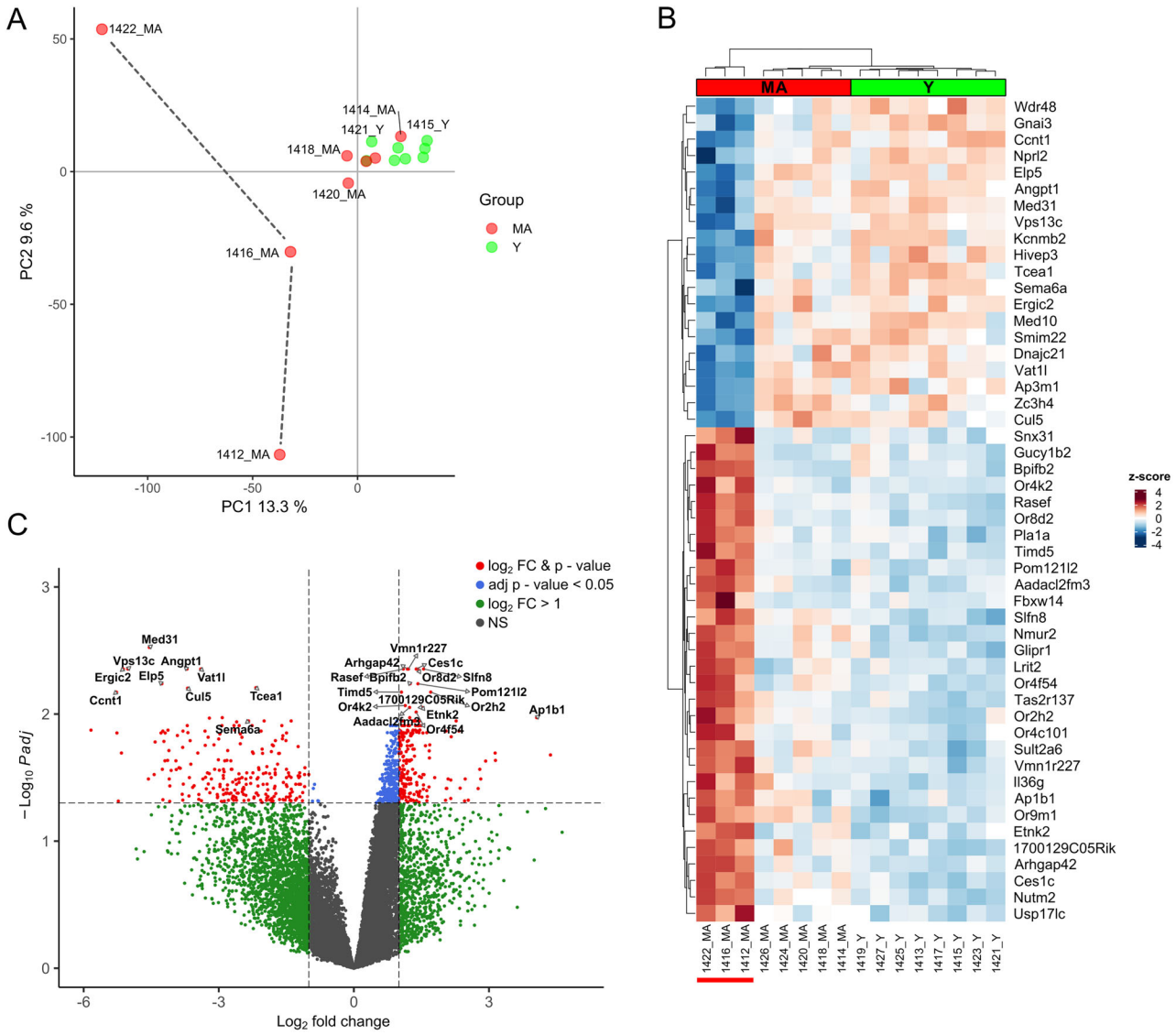

Figure 1. Microarray data analysis uncovers a subset of samples in the MA group. ***A***, PCA of the normalized gene expression values of the microarray dataset, involving eight MA (red dots) and eight young (Y, green dots) GnRH samples. Three MA samples (dotted lines) exhibit separation from the other samples. ***B***, Heat map with hierarchical clustering shows the top 50 DEGs in eight young (sample names ending in Y) and eight middle-aged (sample names ending in MA) samples. Three of the eight MA samples exhibit separation (the red line under the columns) from the remaining five, which display gene expression patterns comparable with those of the Y group. Every row denotes a single gene, and every column denotes a sample. The expression levels are represented by color hues. ***C***, Volcano plot displaying 458 genes with differential expression (DE). Individual genes are represented by dots. The FC in gene expression is displayed on the *x* axis, while the statistical significance of the differences is displayed on the *y* axis. Adjusted $p < 0.05$ and absolute log2 (FC) value >1 were applied to identify DE genes. The statistics of the top 50 DE genes are detailed in Extended Data Figures 1-3 and 1-4. For additional data see Extended Data Figures 1-1 and 1-2.

ORA explores biological processes altered in MA-GnRH neurons

ORA identified significant biological processes (BP) and pathways associated with aging in MA mice (Fig. 2). Downregulated genes ($n = 233$) were enriched in transcription elongation (GO:0006354; $q = 0.0013$), autophagy (GO:0006914; $q = 0.012$), and components of the ubiquitin ligase complex (GO:0000151; $q = 0.0346$) and spliceosomal snRNP complex (GO:0097525; $q = 0.0346$; Fig. 2*A*,*B*). Among upregulated genes ($n = 225$), odorant binding (GO:0005549; $q = 4.11 \times 10^{-10}$) was significantly enriched (Fig. 2*C*,*D*), linking GnRH neurons to olfactory system adaptations during aging. The ORA of the down- and upregulated genes is provided in Extended Data Figure 2-1.

GSEA identifies differentially regulated biological pathways in MA-GnRH neurons

GSEA identified significantly regulated pathways (Fig. 3). Downregulated pathways included mRNA processing (WP310; $q = 1.71 \times 10^{-14}$) and oxidative phosphorylation (WP1248;

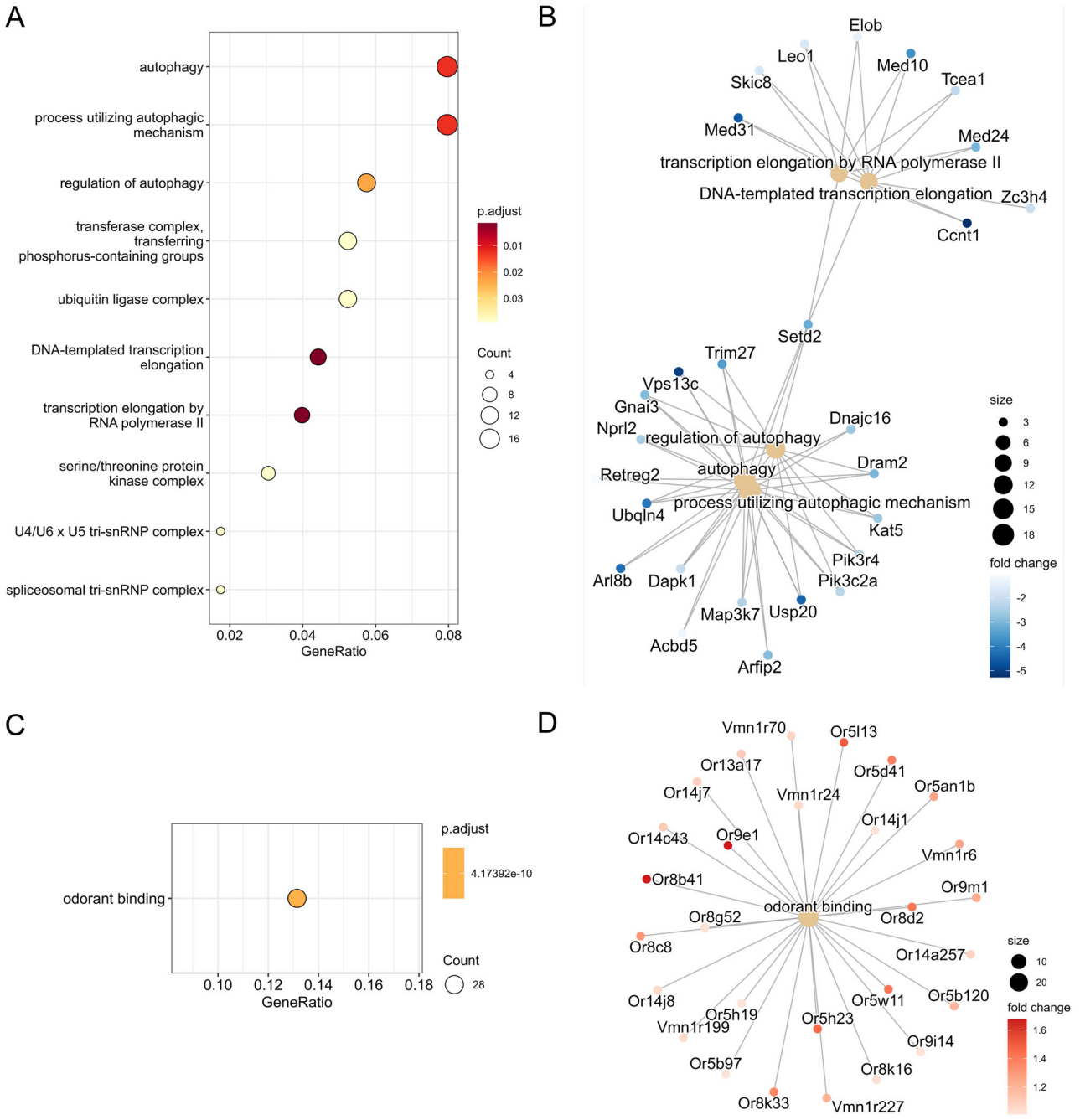

Figure 2. GO term enrichment analysis. ***A***, The downregulated genes in the MA group ($n = 233$) in the ORA unveiled biological processes (BP, i.e., GO:0006368: transcription elongation; GO:0010506 regulation of autophagy) and cellular component (CC, i.e., GO:0000151 ubiquitin ligase complex; GO:0097525 spliceosomal snRNP complex) that are significantly implicated in the MA-GnRH neuron phenotype. ***B***, Network plot of the top five GO terms after the overrepresentation test (ORA) on the 225 downregulated genes depicting the linkages of individual genes and the terms. Selection criteria for the downregulated genes: $\log_2$ FC < 1; adjusted $p < 0.05$ after BH correction. ***C***, Dot plot representation of odorant binding (GO:0005549, molecular function) as a sole significant term, after ORA on the 225 upregulated genes. Selection criteria for upregulated genes: adjusted $p < 0.05$; $\log_2$ FC > 1. ***D***, The upregulated genes overrepresented in the GO (MF) term odorant binding are visualized also as network plot to show the individual genes. Selection criteria for upregulated genes: $\log_2$ FC > 1; adjusted $p < 0.05$ after BH correction. For the statistics of the GO analysis, see Extended Data Figure 2-1.

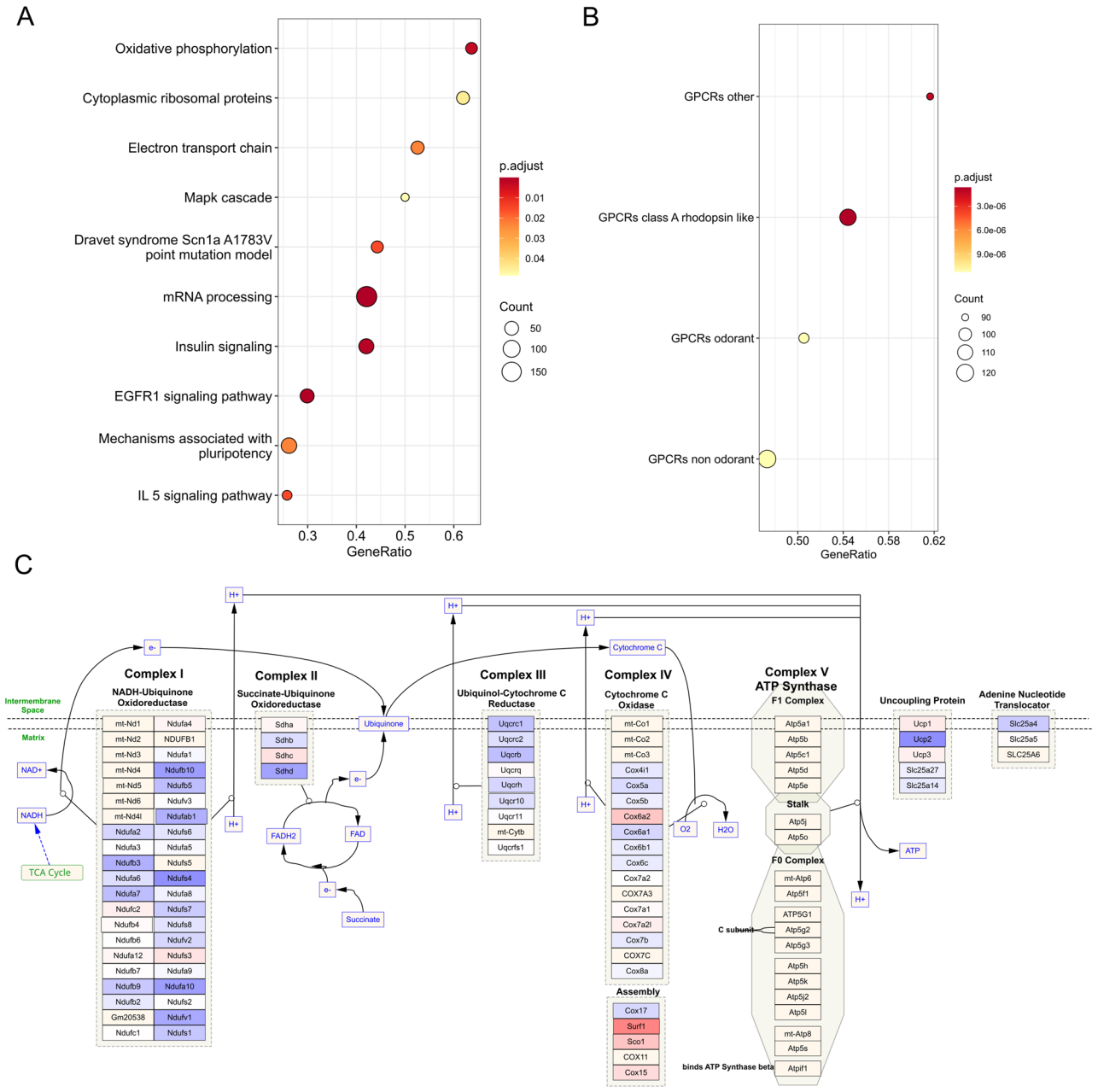

Figure 3. GSEA using WikiPathways. ***A***, The dot plot represents the significantly downregulated (***A***) and upregulated (***B***) pathways. Network Enrichment Score (NES) > |0.5|, adjusted $p < 0.05$. **C**. The significant WP295 electron transport chain pathway (adj $p = 2.27 \times 10^{-02}$) involves several downregulated genes in the mitochondrial respiratory complex I and complex III. For the statistics of the pathway analysis, see Extended Data Figures 3-1 and 3-2.

$q = 1.02 \times 10^{-5}$), indicating a decline in mRNA turnover and ATP production. Upregulated pathways included G-protein–coupled receptor (GPCR)-related signaling, particularly GPCR Class-A Rhodopsin-like receptors (WP189; $q = 3.96 \times 10^{-9}$), indicating altered GnRH neuron signal transduction during reproductive senescence. The statistics of the down- and upregulated pathways are shown in Extended Data Figures 3-1 and 3-2, respectively.

Differential expression of genes controlling excitability and activity of GnRH neurons

Ion channels play a crucial role in shaping neuronal activity, including spike generation and the configuration of firing patterns. Several genes encoding voltage-gated ion channels exhibited marked upregulation in MA-GnRH neurons, including the voltage-gated sodium channel (Scna4), voltage-dependent calcium channel (Cacna1f), voltage-gated potassium channel (Kcna7), and inwardly rectifying potassium channel (Kcnj15; Table 3). Conversely, Kcnj10, another inwardly rectifying potassium channel gene, and Kcnmb2, which encodes a subunit of the large-conductance calcium–activated potassium channel, were significantly downregulated (Table 3).

In addition to ion channels, ionotropic neurotransmitter receptors involved in GnRH neuron regulation displayed altered expression in MA mice. Genes encoding the $GABA_A$ receptor ($GABA_A$-R) subunit beta 1 (*Gabrb1*), nicotinic cholinergic receptor beta 4 polypeptide subunit (*Chrnb4*), and kainate-type glutamate receptor 5 (*Grik5*) were all significantly downregulated (Table 3). Furthermore, genes encoding metabotropic receptors

Table 3. Differential expression of genes encoding certain calcium/sodium/potassium ion channels, neurotransmitter, and neuropeptide receptors in GnRH neurons of MA mice

Entrez ID	Gene symbol	Description	Avg exprs (log2)	FC	*p* val	FDR *p* val
Calcium/potassium/sodium channels						
54,652	*Cacna1f*	Calcium channel, voltage-dependent, alpha 1F subunit	4.94	1.7	5.00×10^{-4}	0.028
110,880	*Scn4a*	Sodium channel, voltage-gated, type IV, alpha	5.62	2.0	3.89×10^{-5}	0.012
16,495	*Kcna7*	Potassium voltage-gated channel, shaker-related subfamily, member 7	5.02	1.8	2.00×10^{-4}	0.018
16,516	*Kcnj15*	Potassium inwardly rectifying channel, subfamily J, member 15	4.51	1.6	8.00×10^{-4}	0.031
16,513	***Kcnj10***	**Potassium inwardly rectifying channel, subfamily J, member 10**	11.11	**−6.2**	6.00×10^{-4}	0.029
72,413	***Kcnmb2***	**Potassium large conductance calcium-activated channel, subfamily M, beta member 2**	12.38	**−7.7**	2.55×10^{-5}	0.011
Neurotransmitter receptors						
108,015	***Chrnb4***	**Cholinergic receptor, nicotinic, beta polypeptide 4**	11.19	**−36.0**	2.30×10^{-3}	0.048
14,400	***Gabrb1***	**$GABA_A$-R, subunit beta 1**	8.43	**−6.0**	1.10×10^{-3}	0.036
14,809	***Grik5***	**Glutamate receptor, ionotropic, kainate 5 (gamma 2)**	13.90	**−1.6**	7.00×10^{-4}	0.031
Neuropeptide receptors						
104,443	*Npffr2*	Neuropeptide FF receptor 2	5.62	2.2	4.00×10^{-4}	0.024
216,749	*Nmur2*	Neuromedin U receptor 2	6.64	2.1	1.38×10^{-5}	0.010
17,203	*Mc5r*	Melanocortin 5 receptor	5.28	2.0	1.00×10^{-3}	0.034
14,715	*Gnrhr*	Gonadotropin-releasing hormone receptor	5.73	1.9	3.00×10^{-4}	0.021
18,160	*Npr1*	Natriuretic peptide receptor 1	5.42	1.8	1.80×10^{-3}	0.043
213,527	*Pth2r*	Parathyroid hormone 2 receptor	5.68	1.8	2.20×10^{-3}	0.047
17,200	*Mc2r*	Melanocortin 2 receptor	5.43	1.8	1.80×10^{-3}	0.043

Selection criterion: FC ≥1.6. The downregulated genes are depicted in bold. For additional data, see Extended Data Figures 1-1–1-4, 2-1, 3-1, and 3-2.

mediating the effects of neuropeptides known to regulate GnRH neurons exhibited distinct alterations with aging. Notably, *Npffr2* (neuropeptide FF receptor 2), *Nmur2* (neuromedin U receptor 2), *Mc2r* and *Mc5r* (melanocortin receptors 2 and 5), *Gnrhr* (GnRH-R), *Npr1* (natriuretic peptide receptor 1), and *Pth2r* (parathyroid hormone 2 receptor) were all significantly upregulated (Table 3).

Electrophysiological features of MA-GnRH neurons

Firing characteristics and passive properties of MA-GnRH neurons

Initially, we characterized the firing parameters of GnRH neurons using current-clamp recordings in acute brain slices from MA mice and young mice. We identified 32 spontaneously firing (80%) and 8 silent (20%) neurons in MA mice and 17 firing (74%) and 6 silent (26%) neurons in young mice. The most notable observation was that the average firing rate of active cells in MA mice was significantly higher than that in young mice (Y, 1.7 ± 0.33 Hz vs MA, 3.4 ± 0.40 Hz; Fig. 4*A–C*; Table 4; $p = 0.0052$; $U = 141$; sum of ranks = 294,931; Mann–Whitney test; Y, $n = 17$; MA, $n = 32$). The frequency histogram of GnRH neurons from young and MA mice (Fig. 4*D*) revealed the presence of a subset of neurons with high firing rates in MA mice, which was absent in young mice. Furthermore, the histogram for MA mice exhibited a local minimum at ∼3.5–4 Hz, suggesting that the MA-GnRH neuron population comprises two subpopulations. To investigate this, we conducted a cluster analysis, and the statistical assessment confirmed two significantly distinct clusters (Cluster 1 vs Cluster 2, Mann–Whitney test, $p = 0.00000236$; Fig. 4*E*; Extended Data Fig. 4-1).

Further analysis showed that the lower firing rate subgroup of MA mice (Cluster 1, 1.8 ± 0.19 Hz) did not differ significantly from the young mice (Cluster 1 vs Y, Mann–Whitney test, $p = 0.4282$; Extended Data Fig. 4-1). Conversely, the higher firing rate subgroup (Cluster 2, 5.8 ± 0.37 Hz) exhibited a significant difference compared with the young group (Cluster 2 vs Y, Mann–Whitney test, $p = 0.0000003173$; Extended Data Fig. 4-1). Next, we examined passive properties (input resistance R_{in}, capacitance, resting potential V_m) and various AP characteristics using current-clamp measurements. A negative square pulse (−60 pA) was applied to assess passive properties, such as R_{in} (Fig. 4*F*) and a positive square pulse (+15 pA) to evaluate parameters of APs in GnRH neurons from young and MA mice (Fig. 4*J,K*). Ten pulses of current steps (−60 to +75 pA in increments of +15 pA, width of 300 ms) was applied to assess evoked firing rates. The graph of the baseline V_m versus current injection steps showed no significant difference between young and MA-GnRH neurons (Fig. 4*G*, comparative linear regression; $p = 0.7348$; DFn = 1; DFd = 206; $F = 0.1150$). In contrast, the evoked firing rate was significantly higher in MA-GnRH neurons than in young ones, when this parameter was graphed against the baseline V_m (comparative linear regression, $p = 0.0001$; DFn = 1; DFd = 216; $F = 29.08$) or the injected current steps (comparative linear regression, $p = 0.0001$; DFn = 1; DFd = 216; $F = 50.04$; Fig. 4*H–I*). The AP amplitude was significantly greater in MA mice (Y 77 ± 4.0 mV vs MA 96 ± 2.4 mV; Student's *t* test $p = 0.0001$; $t = 4.297$; df = 43; 95% confidence interval, −28.11 to −10.15 mV; young, $n = 14$; MA, $n = 31$), whereas the AP half-width was significantly shorter (Y 2 ± 0.31 ms vs MA 1.2 ± 0.052 ms; Student's *t* test $p = 0.0015$; $t = 3.393$; df = 43; 95% confidence interval, 0.2985–1.173 ms; Y, $n = 14$; MA, $n = 31$). The amplitude of AHP was significantly higher in MA mice than in young mice (AHP, Y −14 ± 1.9 mV vs MA −37 ± 1.8 mV; Student's *t* test $p = 0.0001$; $t = 7.574$; df = 43; 95% confidence interval, 16.75–28.90 mV; Y, $n = 14$; MA, $n = 31$; Fig. 4*J,K*; Table 4). However, no significant differences were observed in resting potential, input resistance, or capacitance between young and MA mice (V_m, $p = 0.4798$; $t = 0.7122$; df = 48; 95% confidence interval, −4.877 to 10.23 mV; Y, $n = 14$; MA, $n = 36$; R_{in}, $p = 0.6310$; $t = 0.4870$; df = 22; 95% confidence interval, −164.5 to 265.4 MΩ; Y, $n = 7$; MA, $n = 17$; C_m, $p = 0.5488$; $t = 0.6089$; df = 22; 95% confidence interval, −5.904 to 10.81 pF; Y, $n = 7$; MA, $n = 17$; Student's *t* test; Fig. 4*F*; Table 4). Threshold of APs also showed no significant difference between young and MA-GnRH neurons (Y, −53.3 ± 2.21 mV; $n = 7$; MA, −56.5 ± 1.21 mV; $n = 14$; Student's *t* test; $t = 1.395$; df = 19; $p = 0.1791$; 95% confidence interval, −8.045 to 1.610 mV).

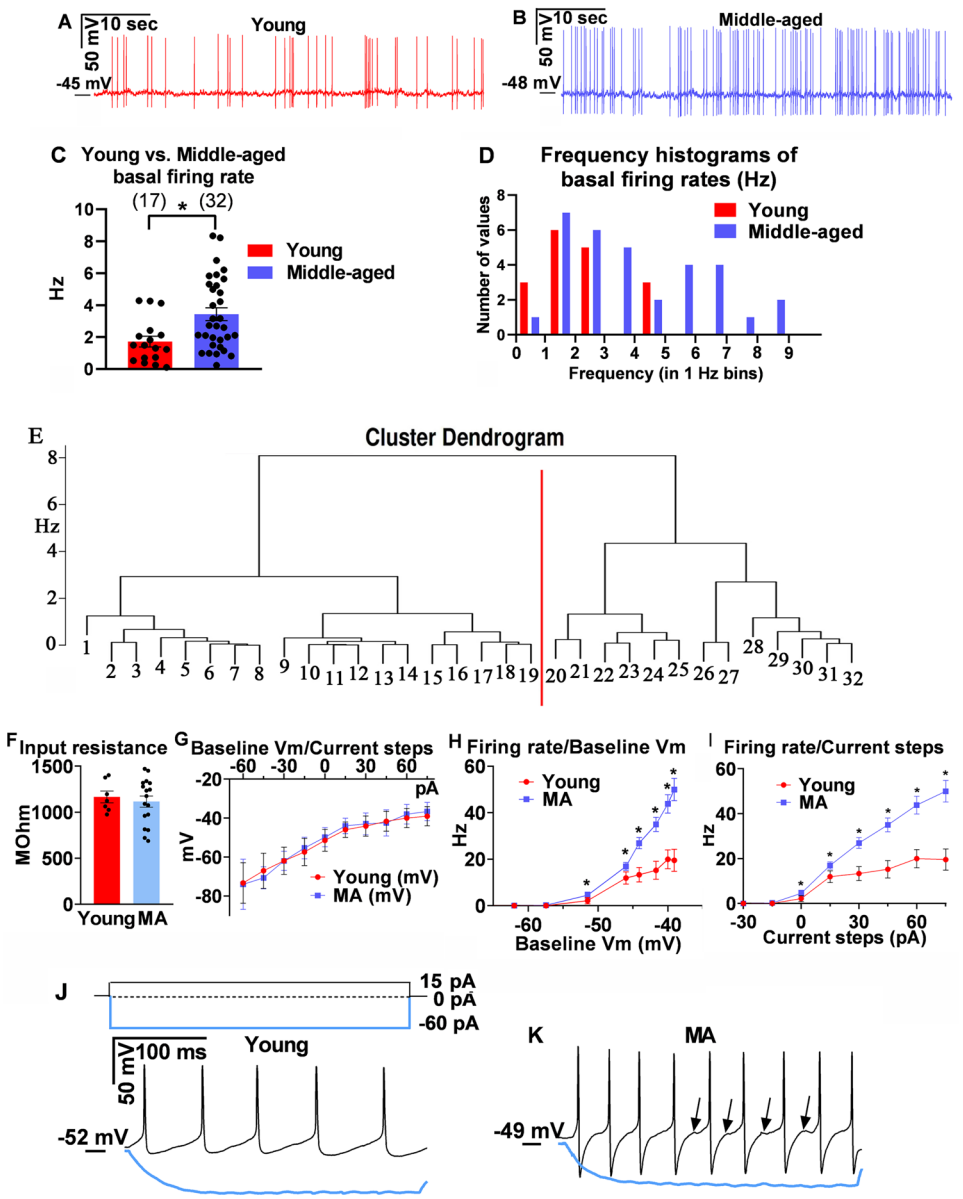

Figure 4. Spontaneous and evoked firing of GnRH neurons of acute brain slices from young diestrous and MA female mice. ***A***, Representative recording of spontaneous firing of a GnRH neuron from a young female mouse. ***B***, Representative recording of firing of a GnRH neuron from a MA female mouse. Note the higher firing rate and presence of the more marked AHP compared with those of young ones in ***A***. ***C***, Bar graph reveals significant difference between the spontaneous firing rate of GnRH neurons from young versus MA mice ($p = 0.0052$ Mann–Whitney test; Y, $n = 17$; MA, $n = 32$). ***D***, Frequency histograms of the firing rate of GnRH neurons of young (red) and MA (blue) mice suggest that the young mouse group consists of a single, homogenous cell population; meanwhile the two, distinct peaks seen in the MA mouse group indicate a functionally heterogeneous GnRH cell population. ***E***, Frequency-distance dendrogram of the spontaneous firing rates of the two cell clusters of the MA mouse group (Cluster 1 vs Cluster 2, $p = 0.00000236$; Cluster 1 vs Y, $p = 0.4282$; Cluster 2 vs Y, $p = 0.0000003173$; Mann–Whitney test). The borderline separating the two clusters is represented by a vertical red line, the lower firing rate cluster is on the left of the red line (cell No. 1–19), and the cluster of the high firing rate is on the right side (cell No. 20–32). ***F***, Input resistance graph shows no significant difference between young ($n = 7$) versus MA ($n = 17$) GnRH neurons (Student's t test $p = 0.6310$). ***G***, The baseline membrane potential (V_m) is graphed against the current injection step in both young ($n = 7$) and MA ($n = 15$) GnRH neurons. The graphs present no significant difference in any step (comparative linear regression; $p = 0.7348$; DFn = 1; DFd = 206; $F = 0.1150$). ***H***, Rate of the evoked firing is graphed against the V_m responding to the current steps. The graph shows that firing activity of MA-GnRH ($n = 15$) neurons was significantly higher than that of young ($n = 7$) GnRH neurons (comparative linear regression; $p = 0.0001$; DFn = 1; DFd = 216; $F = 29.08$). ***I***, Similar scenario was observed when evoked firing rate was graphed against the currents injection steps, firing rate was significantly higher in MA-GnRH neurons (comparative linear regression; $p = 0.0001$; DFn = 1; DFd = 216; $F = 50.04$). ***J, K***, Membrane potential responses of GnRH neurons from young (***J***) and MA (***K***) mice to depolarizing and hyperpolarizing current pulses (above the recording in ***J***). Passive responses to hyperpolarizing pulses (represented by blue lines/recordings) show no differences (V_m, $p = 0.4798$; Y, $n = 14$; MA, $n = 36$; R_{in}, $p = 0.6310$; Y, $n = 7$; MA, $n = 17$; C_m, $p = 0.5488$; Y, $n = 7$; MA, $n = 17$; Student's t test). In contrast, depolarizing pulses (black) evoked a higher firing rate and more robust AP (Student's t test $p = 0.0001$; Y, $n = 14$; MA, $n = 31$) and AHP (Student's t test $p = 0.0001$; Y, $n = 14$; MA, $n = 31$) amplitude in MA mice than in young ones. $^*p < 0.05$. For additional data, see Extended Data Figure 4-1.

Alterations in neurotransmitter signaling to MA-GnRH neurons

Voltage-clamp recordings revealed another striking finding: most MA-GnRH neurons (72%; 32 of 45 cells) displayed no mPSCs (Fig. 5*A*), suggesting potential deficits in afferent neurotransmission. In the 28% of neurons that exhibited mPSCs, their activity (1.9 ± 0.26 Hz) was partially reduced by the $GABA_A$-R blocker picrotoxin (100 μM) and fully abolished by the subsequent addition of the broad-spectrum glutamate receptor (Glut-R) inhibitor kynurenic acid (2 mM; Fig. 5*B–D*). These results indicate that mPSCs detected in the minority of GnRH

Table 4. Basic electrophysiological properties of GnRH neurons obtained from brain slice preparations of young and MA female mice

					Mann–Whitney test		
Electrophysiological properties	Young	n/*N* (young)	MA	n/*N* (MA)	Sum of ranks	*U*	*p*
Spontaneous firing rate	1.7 ± 0.33 Hz	17/3	3.4 ± 0.40 Hz	32/8	294,931	141	0.0052*
					Student's *t* test		
					t	*df*	*p*
AP amplitude	77 ± 4.0 mV	14/3	96 ± 2.4 mV	31/7	4.297	43	0.0001*
AP duration at 1/2 amplitude	2 ± 0.31 ms	14/3	1.2 ± 0.052 ms	31/7	3.393	43	0.0015*
AHP amplitude	−14 ± 1.9 mV	14/3	−37 ± 1.8 mV	31/7	7.574	43	0.0001*
Resting membrane potential	−48 ± 1.4 mV	14/3	−50.0 ± 2.3 mV	36/7	0.7122	48	0.4798
Input resistance	1,115 ± 65 MΩ	7/2	1,166 ± 88 MΩ	17/7	0.4870	22	0.6310
Membrane capacitance	24 ± 2.9 pF	7/2	21 ± 2.3 pF	17/7	0.6089	22	0.5488

n/N, the number of measured neurons/number of mice; Young, adult diestrous female mice.
*Significant difference. For additional data, see Extended Data Figure 4-1.

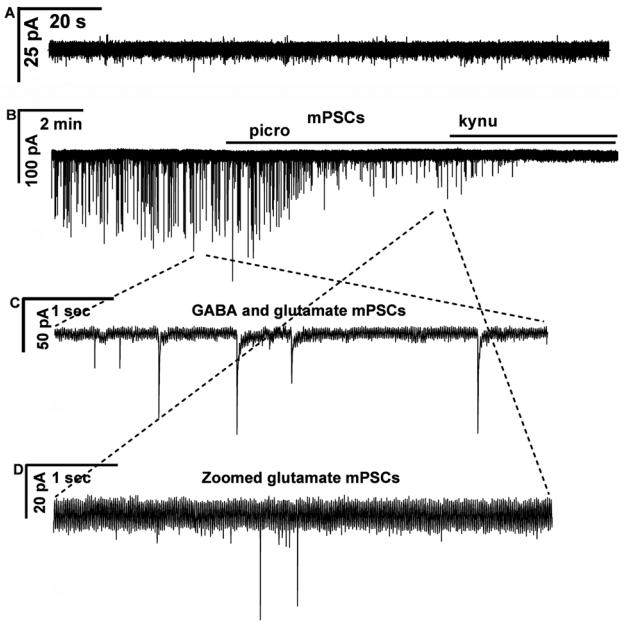

Figure 5. Absence/presence of mPSCs in GnRH neurons of acute brain slices from MA mice. ***A***, Representative recording demonstrates that most GnRH neurons (32 from 45 cells) present no mPSCs. ***B***, Mixed PSCs were observed in the remaining 13 GnRH neurons. These mPSCs present $GABA_A$-R and glutamate-mediated synaptic currents because the $GABA_A$-R blocker picrotoxin (picro) and glutamate-R inhibitor, kynurenic acid (kynu) abolished them. ***C***, Zoomed recording before administration of picrotoxin and kynurenic acid also suggests the presence of both the slower GABAergic and the faster glutamatergic mPSCs. ***D***, In another zoomed recording after applying picrotoxin but before administration of kynurenic acid, picrotoxin has already eliminated the GABAergic mPSCs; however, the fast glutamatergic ones are still present. Horizontal black lines above the recording show administration of picrotoxin and kynurenic acid.

neurons represent both GABAergic and glutamatergic inputs in MA mice.

To determine whether the absence of mPSCs was due to the dysfunction in the input to the recorded GnRH neuron or the recorded GnRH neuron itself, we examined the effects of extracellularly applied GABA (50 μM–1 mM) or glutamate (1 mM) on firing activity in young and MA-GnRH neurons using current-clamp recordings. A single bolus of either neurotransmitter transiently increased the firing rate significantly in both young and MA animals (young ctrl, 1.5 ± 0.42 Hz vs GABA, 4.2 ± 0.79 Hz; $p = 0.0012$; $t = 4.645$; df = 9; 95% confidence interval, 1.361–3.947 Hz; $n = 10$ Student's *t* test; ctrl 0.6 ± 0.11 Hz vs glutamate 3.0 ± 0.57 Hz; $p = 0.008$; $t = 4.964$; df = 9; 95% confidence interval, 1.278–3.418 Hz; $n = 10$ Student's *t* test; MA, ctrl 3.8 ± 0.71 Hz vs GABA 6.5 ± 1.1 Hz; $p = 0.002$; $n = 10$ Wilcoxon test; ctrl 4.0 ± 0.68 Hz vs glutamate 4.8 ± 0.75 Hz; $p = 0.002$; $n = 10$ Wilcoxon test; Fig. 6*A1-2*,*B1-2*; Extended Data Fig. 6-1), indicating that GnRH neurons in MA mice remained responsive to these neurotransmitters. We must note, however, that the dose of GABA (1 mM) effective in MA-GnRH neurons was extremely high impairing them in young ones; therefore, it was necessary to use lower GABA concentration (50 μM) during the measurements. Despite the lower dose, the effect of GABA was still significantly stronger in young GnRH neurons (Fig. 6*E*; Extended Data Fig. 6-1; two-way ANOVA; intercept, $p = 2.2439 \times 10^{-7}$; $F = 64.79630$; df = 1; age factor, $p = 0.02221686$; $F = 6.25985$; df = 1; GABA treatment factor, $p = 0.00005004$; 27.95791; df = 1). Similarly, the action of glutamate was more robust in young mice (Fig. 6*E*; Extended Data Fig. 6-1; two-way ANOVA; intercept, $p = 3.107437 \times 10^{-7}$; $F = 61.89417$; df = 1; age factor, $p = 0.003740929$; $F = 11.07690$; df = 1; glutamate treatment factor, $p = 6.15112178 \times 10^{-6}$; $F = 39.67103$; df = 1). To confirm these observations, we conducted voltage-clamp recordings in the presence of TTX to block APs. Both GABA (500 μM in young and 1 mM in MA) and glutamate (1 mM) elicited inward currents in both young and MA animals (Y, GABA, −1,079 ± 122 pA; Student' *t* test $p = 0.001$; $t = 8.817$; df = 9; 95% confidence interval, −1,356 to −802.4 pA; $n = 10$; glutamate, −148 ± 16 pA; Student' *t* test $p = 0.001$; $t = 9.42$; df = 6; 95% confidence interval, −187.0 to −109.9 pA; $n = 7$; MA, GABA, −346.3 ± 60.8 pA; Student' *t* test $p = 0.0023$; $t = 5.697$; df = 5; 95% confidence interval, −502.6 to −190.1 pA; $n = 6$; glutamate, −75 ± 10.21 pA; Student' *t* test $p = 0.018$; $t = 7.343$; df = 2; 95% confidence interval, −118.9 to −31.05 pA; $n = 3$; Fig. 6*C1-2*,*D1-2*; Extended Data Fig. 6-2), demonstrating that the GABA and Glut-Rs remained functional in the recorded MA-GnRH neurons, however, responsiveness of MA-GnRH neurons was significantly attenuated (Fig. 6*F*; Extended Data Fig. 6-2; GABA, Student's *t* test $p = 0.006$; $t = 4.396$; df = 14; 95% confidence interval, −1,091 to −375.3 pA; glutamate, Student's *t* test $p = 0.021$; $t = 2.863$; df = 8; 95% confidence interval, −132.6 to −14.30 pA). We must note that the intracellular electrode solution was "high-chloride" (140 mM); therefore GABA was excitatory via the $GABA_A$-R.

Using this technique that preserves the native, high intracellular chloride concentration of adult GnRH neurons, $GABA_A$-R activation is depolarizing and can be excitatory (DeFazio et al., 2002; Herbison and Moenter, 2011). Furthermore, we tested the effects of sequentially applied neurotransmitter blockers [picrotoxin, kynurenic acid, atropine (10 μM), and mecamylamine (10 μM)]

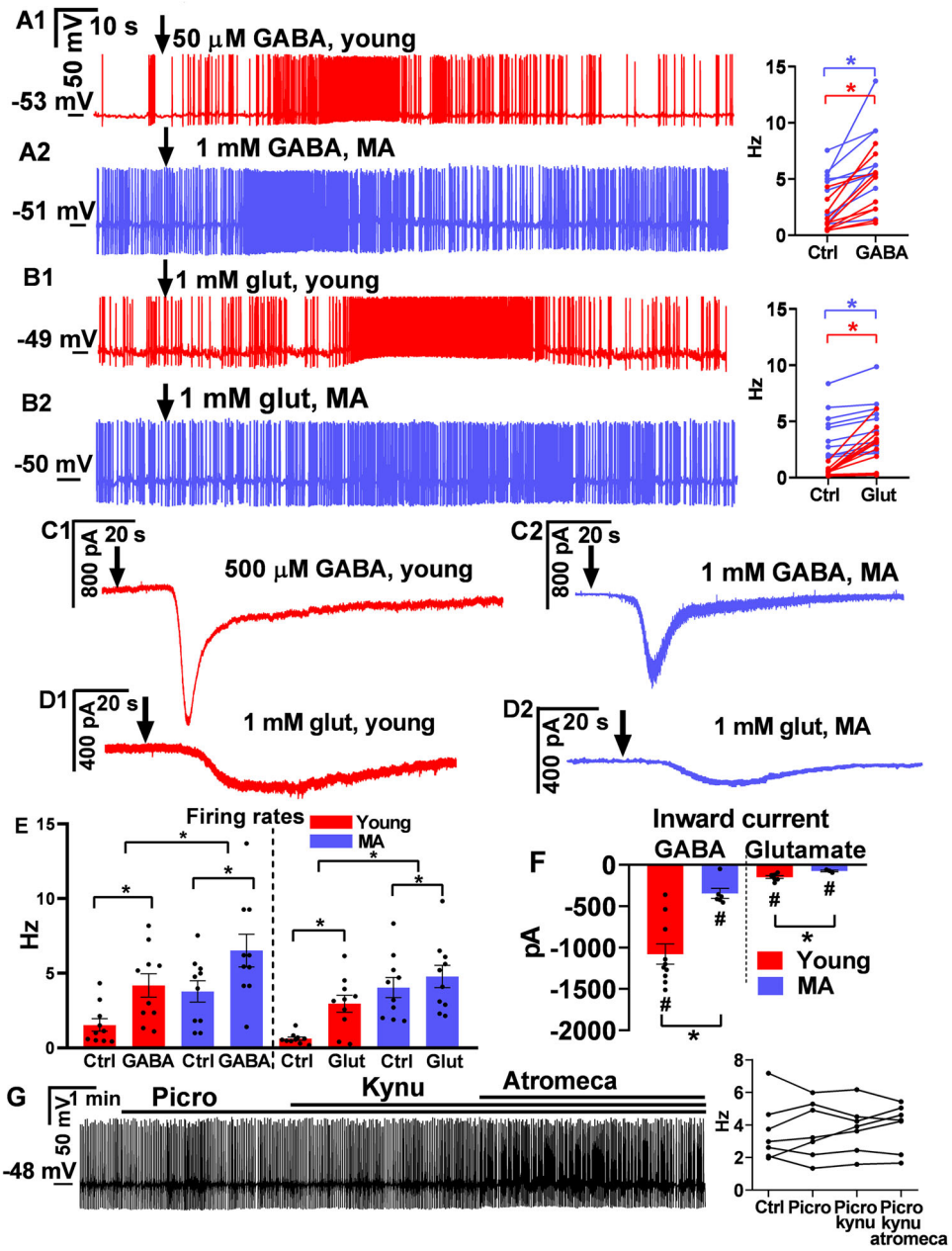

Figure 6. Representative recordings of GABAergic and glutamatergic firing and inward current responses of GnRH neurons in brain slice from young and MA mice. ***A*1,2**, GABA application increases the spontaneous firing rate transiently in both young (red) and MA (blue) samples (Y ctrl 1.5 ± 0.42 Hz vs GABA 4.2 ± 0.79 Hz; $p = 0.0012$; $n = 10$; Student's t test; MA, ctrl 3.8 ± 0.71 Hz vs GABA 6.5 ± 1.1 Hz; $p = 0.002$; $n = 10$ Wilcoxon test); however, the effect of GABA is more robust in young ones (2-way ANOVA; intercept, $p = 2.2439 \times 10^{-7}$; age factor, $p = 0.02221686$; GABA treatment factor, $p = 0.00005004$). We have to note that the intracellular electrode solution was "high-chloride"; therefore GABA was excitatory via the $GABA_A$-R. Using this technique that preserves the native high intracellular chloride concentration, $GABA_A$-R activation is depolarizing and can be excitatory in adult GnRH neurons. ***B*1,2**, Glutamate administration also elevates the firing rate in both young (red) and MA-GnRH (blue) neurons (Y ctrl 0.6 ± 0.11 Hz vs glutamate 3.0 ± 0.57 Hz; $p = 0.008$; $n = 10$ Student's t test; MA ctrl 4.0 ± 0.68 Hz vs glutamate 4.8 ± 0.75 Hz; $p = 0.002$; $n = 10$ Wilcoxon test); however, the magnitude of the action is stronger in GnRH neurons from young mice (2-way ANOVA; intercept, $p = 3.107437 \times 10^{-7}$; age factor, $p = 0.003740929$; glutamate treatment factor, $p = 6.15112178 \times 10^{-6}$). ***C*1,2**, GABA evokes a robust inward current in GnRH neurons both in young (red) and MA-GnRH (blue) neurons (Y, GABA, −1,079 ± 122 pA; Student' t test $p = 0.001$; $n = 10$; MA, GABA, −346.3 ± 60.8 pA; Student's t test $p = 0.0023$; $n = 6$). The amplitude of the current is larger in young mice (Student's t test $p = 0.006$). ***D*1,2**, Glutamate also induces inward current both in young (red) and MA-GnRH (blue) neurons (Y glutamate, −148 ± 16 pA; Student' t test $p = 0.001$; $n = 7$; MA glutamate, −75 ± 10.21 pA; Student' t test $p = 0.018$; $n = 3$). Like the GABA effect, the amplitude of the inward current evoked by glutamate is larger in young samples (Student's t test $p = 0.021$). ***E***, Summary bar graph of the firing rate changes evoked by GABA or glutamate in young (red) or MA-GnRH (blue) neurons. The effects of both GABA and glutamate are larger in young mice (2-way ANOVA; GABA, intercept, $p = 2.2439 \times 10^{-7}$; age factor, $p = 0.02221686$; GABA treatment factor, $p = 0.00005004$; glutamate, intercept, $p = 3.107437 \times 10^{-7}$; age factor, $p = 0.003740929$; glutamate treatment factor, $p = 6.15112178 \times 10^{-6}$). ***F***, Summary bar graph of the amplitude of the inward current evoked by GABA/glutamate in young (red) or MA-GRH (blue) neurons. The amplitudes are higher in young mice (GABA, $p = 0.006$; glutamate, $p = 0.021$ Student's t test). ***G***, The spontaneous firing rate presents no change upon administration of picrotoxin (picro), kynurenic acid (kynu), and even the cocktail of the acetylcholine receptor blockers atropine/mecamylamine (atromeca), suggesting absence/diminution of spontaneous release of these neurotransmitters to the recorded GnRH neurons (Friedman test $p = 0.9326$; $n = 7$). The arrow shows the administration of the single bolus of GABA or glutamate. Horizontal black lines above the recording show application and continuous presence of picrotoxin, kynurenic acid, atropine, and mecamylamine. $^*p < 0.05$ between two groups (ctrl vs GABA/glutamate in ***A*1,2** and ***B*1,2, *E***, or young vs MA in ***F***), $^{\#}p < 0.05$ between one group versus the unchanged condition (GABA/glutamate vs 0 pA in ***F***). For additional data, see Extended Data Figure 6-1–6-3.

on the spontaneous firing rate of GnRH neurons in MA mice. None of these inhibitors significantly affected firing activity (Fig. 6*G*; Extended Data Fig. 6-3; Friedman test $p = 0.9326$; $n = 7$).

Sustained responsiveness of MA-GnRH neurons to exogenous estradiol

Estradiol (E2) is a potent regulator of female GnRH neurons via positive and negative feedback mechanisms in young animals. Here, we tested the sensitivity of GnRH neurons from MA mice to various concentrations of E2 using the current-clamp method. E2 applied both at low (10 pM) and high (200 pM) doses as a single bolus significantly decreased the firing rate (low dose, ctrl 3.0 ± 0.74 Hz vs E2 2.0 ± 0.44 Hz; Wilcoxon test $p = 0.0319$; $n = 7$; Fig. 7*A*; Extended Data Fig. 7-1. High dose, ctrl 2.8 ± 0.63 Hz vs E2 1.6 ± 0.33 Hz; Wilcoxon test $p = 0.0165$; $n = 7$; Fig. 7*B*; Extended Data Fig. 7-1). These findings indicate that MA-GnRH neurons retain their ability to respond to estradiol.

Neuropeptide signaling via GPCRs: putative role of KP

To further elucidate the potential mechanisms responsible for the increased firing rate of MA-GnRH neurons, various inhibitors were applied while spontaneous firing was recorded using the current-clamp method. First, the membrane-impermeable GPCR blocker GDP-β-S (2 mM) was added to the intracellular solution in the recording electrode. Administration of GDP-β-S significantly reduced the firing rate within 15 min (1st minute 3.3 ± 0.61 Hz vs 15th minute 0.94 ± 0.34 Hz; $p = 0.0159$; $n = 7$ Wilcoxon test; Fig. 8*A*; Extended Data Fig. 8-1), suggesting a fundamental role of GPCR-mediated actions in maintaining the high firing rate. We then targeted two GPCRs highly expressed in GnRH neurons, the GnRH and KP-R. The GnRH-R blocker, Antide (100 nM), did not induce any significant change in the firing rate (ctrl, 3.8 ± 0.53 Hz vs Antide, 3.9 ± 0.64 Hz; $p = 0.9375$; $n = 6$ Wilcoxon test; Fig. 8*B*; Extended Data Fig. 8-1). However, extracellular administration of KP (200 nM) as a single bolus evoked a robust increase in the firing rate of both young and MA-GnRH neurons (Y 1.2 ± 0.07 Hz vs KP 3.6 ± 0.60 Hz; $p = 0.0073$; $t = 3.983$; df = 6; 95% confidence interval, 0.9086–3.803 Hz; $n = 7$; Student's t test; MA, ctrl 4.3 ± 1.0 Hz vs KP 6.7 ± 1.6 Hz; $p = 0.0156$; $n = 7$ Wilcoxon test; Fig. 8*C*1-2; Extended Data Fig. 8-1); however, the effect seemed somewhat lower in MA mice (Fig. 8*E*; Extended Data Fig. 8-1; two-way ANOVA; intercept, $p = 0.00006319$; $F = 35.8724$; df = 1; age factor, $p = 0.03663636$; $F = 5.52788$; df = 1; KP treatment factor, $p = 0.00024316$; $F = 26.4665$; df = 1). Moreover, the KP-R antagonist, KP-234 (10 nM), triggered no significant effect in young mice (ctrl, 1.3 ± 0.13 Hz vs KP-234, 1.4 ± 0.15 Hz; $p = 0.721$; $t = 0.3744$; df = 6; 95% confidence interval, −0.3875 to 0.5275 Hz; $n = 7$ Student's t test; Fig. 8*D*1; Extended Data Fig. 8-1), whereas it significantly reduced the spontaneous firing rate in MA-GnRH neurons (ctrl, 4.6 ± 1.2 Hz vs KP-234, 3.0 ± 0.87 Hz; $p = 0.0234$; $n = 8$ Wilcoxon test; Fig. 8*D*2; Extended Data Fig. 8-1) suggesting a tonic KP release mechanism from the terminals of the afferents to MA-GnRH neurons. Summary bar graph confirms these observations (Fig. 8*E*; Extended Data Fig. 8-1; two-way ANOVA; intercept, $p = 0.000436$; $F = 21.8359$; df = 1; age factor, $p = 0.045982$; $F = 4.86669$; df = 1; KP-234 treatment factor, $p = 0.041149$; $F = 5.136114$; df = 1). These findings highlight the involvement of the KP system in regulating the high firing rate of GnRH neurons in MA mice

Figure 7. Effect of 17β-estradiol (E2) on spontaneous firing rate of GnRH neurons from MA female mice. ***A***, Single bolus of low dose of E2 (10 pM, arrow) decreases the firing rate transiently, suggesting that the negative feedback mechanism is still operational at middle age (ctrl 3.0 ± 0.74 Hz vs E2 2.0 ± 0.44 Hz; Wilcoxon test $p = 0.0319$; $n = 7$). ***B***, Higher dose of E2 (200 pM) also diminished the firing rate (ctrl 2.8 ± 0.63 Hz vs E2 1.6 ± 0.33 Hz; Wilcoxon test $p = 0.0165$; $n = 7$). *$p < 0.05$. For additional data, see Extended Data Figure 7-1.

Strength and limitations of applied technical approaches

Transcriptomics

Our LCM-based microarray analysis represents a high-throughput transcriptomic study aimed at identifying cell-type–specific alterations in gene expression. The fixation of ribonucleoproteins in tissue samples facilitates a snapshot-like acquisition of information. The study provides average expression levels of all neurons collected and pooled per animal, detecting only the vector of the gene expression change, indicating both its magnitude (FC) and direction (up- or downregulation). Therefore, robust, unidirectional changes and pathways (i.e., mRNA processing, autophagy) are much easier to detect. However, this approach does not allow the analysis of variability at the individual cellular level, thereby concealing gene expressions that exhibit high cell-to-cell variability.

Slice electrophysiology

Slice electrophysiology of neurons tagged with green fluorescent protein in genetically modified mice provides a robust tool to study electric responses of identified, in this case, GnRH neurons. Using this method, the experimenter can change the selected drugs (E2, GABA, glutamate, KP, etc.) applied to the cells rapidly with the exact timing of onset of their administration. Using this technique, we were able to demonstrate the functional heterogeneity of MA-GnRH neuron population, the increased firing rate of the cells, their impaired GABA/glutamatergic regulation, the tonic KP release, and sustained responsiveness to E2. As a limitation of the in vitro technique, one should keep in mind that the acute slice preparation is isolated from the rest of the brain. The loss of its neuronal afferents and hormonal inputs, therefore, may modify the cellular responses and basic electric properties of its targeted neurons.

Discussion

We identified significant alterations in gene expression and electrophysiological activity of GnRH neurons in MA female mice. The principal findings indicate the following: (**1**) In one-third of MA mice, GnRH neurons displayed differentially expressed, upregulated genes linked to immune signaling and odorant perception, while the main downregulated pathways included mRNA processing, oxidative phosphorylation, electron transport, and estrogen signaling. (**2**) Genes coding for certain $GABA_A$, glutamate and nicotinic acetylcholine receptor subunits were downregulated, contrasting various upregulated neuropeptide receptor genes. (**3**) Genes encoding certain sodium,

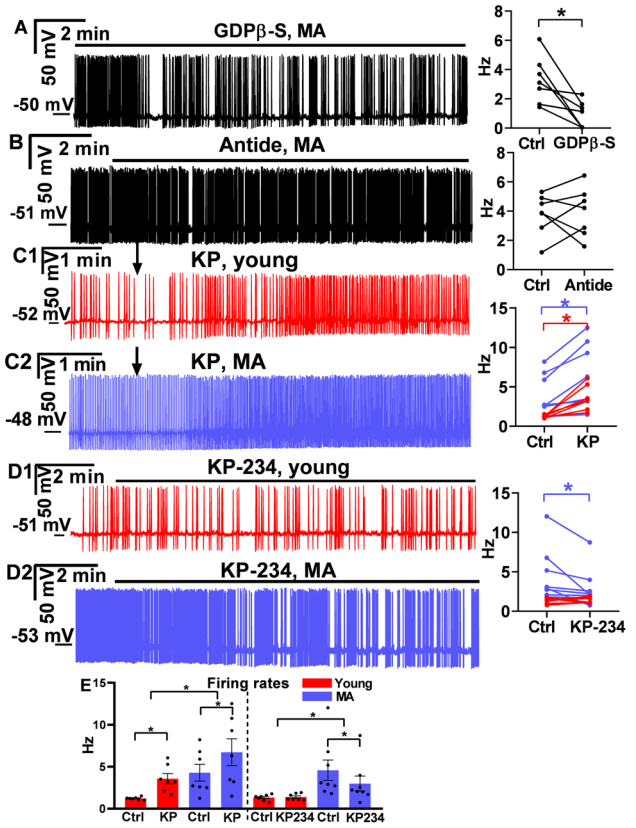

Figure 8. Representative recordings of spontaneous firing of GnRH neurons in MA mice upon administration of various agonists and antagonists. ***A***, The intracellularly applied G-protein inhibitor, GDP-β-S, decreased the firing rate ($p = 0.0159$; $n = 7$ Wilcoxon test) suggesting a regulatory role of G-proteins in the enhanced firing rate of GnRH neurons in MA mice. ***B***, Antagonist of the G-protein–coupled GnRH receptor, Antide, evoked no response in the firing rate (ctrl 3.8 ± 0.53 Hz vs Antide 3.9 ± 0.64 Hz; $p = 0.9375$; $n = 6$ Wilcoxon test). ***C1,2***, KP elevated firing rate in both young (red) and MA-GnRH (blue) neurons showing that these cells possess the full machinery to respond to KP (Y 1.2 ± 0.07 Hz vs KP 3.6 ± 0.60 Hz; $p = 0.0073$; $n = 6$ Student's t test; MA, ctrl 4.3 ± 1.0 Hz vs KP 6.7 ± 1.6 Hz; $p = 0.0156$; $n = 7$; Wilcoxon test) although the effect seems somewhat lower in MA (2-way ANOVA; intercept, $p = 0.00006319$; age factor, $p = 0.03663636$; KP treatment factor, $p = 0.00024316$). ***D1,2***, The G-protein–coupled KP-R antagonist, KP-234, evoked no effect in young GnRH neurons (red, ctrl 1.3 ± 0.13 Hz vs KP-234 1.4 ± 0.15 Hz; $p = 0.721$; $n = 6$ Student's t test) but decreased the firing rate in MA samples (blue, ctrl 4.6 ± 1.2 Hz vs KP-234 3.0 ± 0.87 Hz; $p = 0.0234$; $n = 8$; Wilcoxon test) indicating a continuous, tonic KP input to MA-GnRH neurons that might contribute to the high firing rate. ***E***, Summary bar graph of the firing rate changes evoked by KP or KP234 in young (red) or MA-GnRH (blue) neurons. KP evoked a somewhat larger effect in young mice (2-way ANOVA; intercept, $p = 0.00006319$; age factor, $p = 0.03663636$; KP treatment factor, $p = 0.00024316$); however, KP234 acted in MA mice only (2-way ANOVA; intercept, $p = 0.000436$; age factor, $p = 0.045982$; KP-234 treatment factor, $p = 0.041149$). The arrow shows administration of the single bolus of KP. The horizontal black lines above the recordings show application and continuous presence of the various blockers. *$p < 0.05$ between two groups (ctrl vs GDP-β-S/Antide/KP/KP-234 in ***A***, ***B***, ***C1,2***, ***D1,2***, or ***E***). For additional data, see Extended Data Figure 8-1.

potassium, and calcium ion channels, known regulators of neuron excitability, were also differentially expressed in MA-GnRH neurons. (**4**) At middle age, the GnRH cells showed an increased firing rate and either the complete absence or marked reduction of mPSCs. (**5**) They displayed excitatory responses to exogenous GABA, glutamate, and KP administration. (**6**) Unlike young GnRH neurons, the MA cells received a tonic KP regulation. (**7**) Exposure to exogenous estradiol inhibited their activity.

In the transcriptome study, the appearance of the MA3 and MA5 clusters in the MA group highlights the heterogeneity of the animals and their GnRH neurons. No DEGs were identified when comparing the MA5 subgroup with the young group; therefore, the MA5 subgroup was excluded from further analysis. In contrast, the MA3 subgroup displayed a substantial number of DEGs and was used for further downstream analysis.

ORA of the upregulated genes showed significant association with odorant binding, suggesting that olfactory cues may influence GnRH neuron function during reproductive senescence. Correspondingly, GSEA identified several upregulated pathways involving GPCRs. The upregulation of GPCR pathways, including those related to rhodopsin-like and odorant receptors, suggests enhanced signal transduction mechanisms in GnRH neurons, potentially representing a compensatory response to maintain GnRH neuron function during reproductive senescence.

Downregulated genes were significantly enriched in processes such as transcription elongation, autophagy, and components of the ubiquitin ligase and spliceosomal snRNP complexes. These findings suggest that aging may impair transcriptional regulation, protein degradation, and RNA splicing in GnRH neurons, potentially contributing to age-related physiological changes. A meta-analysis identified common molecular signatures of aging, including significant gene expression changes, downregulation of genes associated with mitochondrial function, and oxidative phosphorylation (de Magalhães et al., 2009).

In our GSEA, the most significantly downregulated pathway was mRNA processing, highlighting a decline in RNA turnover and synthesis with age. Pathways related to oxidative phosphorylation, cytoplasmic ribosomal proteins, and the electron transport chain were also downregulated, indicating reduction in energy metabolism and ATP production. Aging impacts critical biological processes such as mitochondrial function and translation in a tissue-specific manner in humans (Yamamoto et al., 2022). The identified regulated pathways in various neurons confirm that genome-wide expression changes in MA-GnRH neurons are partly attributable to age-related alterations, emphasizing the vulnerability of GnRH neurons to disruptions of the homeostatic mechanisms essential for neuronal health.

The differential expression of particular sodium, potassium, and calcium ion channel genes, downregulation of $GABA_A$, kainate and acetylcholine receptor subunit genes, and upregulation of genes encoding various neuropeptide receptors in MA-GnRH neurons were indicative of functional changes in the activity of the cells that were explored by electrophysiology.

As hallmark, a significant threefold increase in the firing rate was observed in a subpopulation of MA-GnRH neurons. Age-dependent changes in various neuronal features have been previously reported (Rizzo et al., 2014). Firing rates also change with age (Yan et al., 2003; Chang et al., 2005; Randall et al., 2012). In contrast to our findings, isolated GnRH neurons from ovariectomized or E2-substituted MA mice showed decreased firing (Wang et al., 2008). It is of note that we used gonadally intact mice, and GnRH neurons were examined in brain slices with partially preserved afferents. Firing rates in GnRH neurons of both young and cluster 1 MA mice were consistent with previously published values (0.8–2.47 Hz; Spergel et al., 1999; Christian et al., 2005; Chu and Moenter, 2005; Christian and Moenter, 2008; Roland and Moenter, 2011; Liu and Herbison, 2013, 2014).

The characteristic burst firing of GnRH neurons (Chu et al., 2012) was observed in MA neurons firing at both low and high frequencies. However, bursts could not be identified in several high-firing MA-GnRH neurons because their interburst periods were absent due to the extremely high firing rates. The amplitude of the AHP was significantly higher in MA-GnRH neurons.

AHPs can contribute to fast spiking by activating T-type Ca-channels (Jaffe and Brenner, 2018). GnRH neurons possess all the ion channels required for AHPs (Spergel et al., 1996; Hu et al., 2006; Hiraizumi et al., 2008; Liu and Herbison, 2008) and also the T-type Ca-channels (Rønnekleiv et al., 2012, 2015). Therefore, it is reasonable to assume a potential causal relationship between the high amplitude of AHPs and the elevated firing rate in MA-GnRH neurons. While optogenetically induced synchronous burst firing alone failed to evoke LH pulse generation in young animals (Campos and Herbison, 2014), elevated GnRH pulse amplitudes have been reported in peri- and postmenopausal nonhuman primates (Gore et al., 2004). In MA male mice, the elevation of LH pulse frequency was observed preceding the later decrease of pulse amplitude (Wang et al., 2021). The heterogeneity observed in the firing rates of MA-GnRH neurons suggests that the transition to reproductive senescence occurs gradually. Age-dependent heterogeneity has also been reported in hippocampal and cortical GABAergic neurons (Rozycka and Liguz-Lecznar, 2017).

The characteristics and frequency of APs are fundamentally regulated by ion conductances (Norberg et al., 2013; Piet and Herbison, 2018; Constantin et al., 2022). The upregulation of the voltage-gated Na-channel subunit gene (Scn4a) may contribute to the rapid depolarizing phase of the AP (Chu and Moenter, 2006). The large-conductance calcium-activated K-channels (BK) influence spontaneous firing by altering the AHP (Womack et al., 2009). The upregulated Kcnmb2 gene suggests ongoing changes in the calcium-sensitivity of BK-currents. Additionally, increased expression of the voltage-dependent Ca-channel subunit (Cacna1f) indicates plausible changes in calcium conductance during middle age.

The diminished GABA and glutamate regulation of MA-GnRH neurons (i.e., the absence of mPSCs in most measured cells) suggests that the production/release of these neurotransmitters is reduced. The diminished inward GABA/glutamate currents suggest attenuated GABA/glutamate receptor function in MA-GnRH neurons. The downregulation of genes encoding $GABA_A$ (*Gabrb1*), and glutamate (*Grik5*) receptor subunits indicates alterations of postsynaptic mechanisms, supporting the electrophysiological observations. Similar age-dependent neurotransmission failures have been observed in basal forebrain and cortical neurons (Wong et al., 2000; Luebke et al., 2004; Griffith et al., 2014). Aging affects both pre- or postsynaptic mechanisms (Rozycka and Liguz-Lecznar, 2017). Reduced or eliminated presynaptic neurotransmitter release has been observed in aging cortical and hippocampal neurons (Ling et al., 2005; Burianova et al., 2009; Gold and Bajo, 2014). Aging may also influence postsynaptic mechanisms by impairing neurotransmitter receptor synthesis and function (Gutiérrez et al., 1996, 1997; Yu et al., 2006; Caspary et al., 2013). It is of note that a minority of MA-GnRH neurons exhibited mPSCs in this study; however, they represented both GABAergic and glutamatergic inputs (Spergel et al., 1999; DeFazio et al., 2002; Christian et al., 2009; Watanabe et al., 2009).

Numerous GPCRs are expressed in GnRH neurons (Xu et al., 2004; Spergel, 2019). Blockade of GPCRs reduced the firing rate, indicating that GPCRs contributed to the high firing rate of MA-GnRH neurons. One of the tested GPCRs was the GnRH-R expressed in GnRH neurons (Xu et al., 2004), but its selective blockade did not affect the firing rate. The other candidate was the KP-R, as hypothalamic KP neurons relay feedback effects of E2 to GnRH neurons (Oakley et al., 2009; Kalló et al., 2012; León et al., 2016; Kauffman, 2022). In MA mice, KP accelerated the firing rate, while the KP antagonist reduced it, confirming the sustained responsiveness of GnRH neurons. Since KP neurons in the arcuate nucleus express estrogen receptors and mediate negative E2 feedback, it is conceivable that declining E2 levels in aging animals alleviate the KP system-mediated inhibition of GnRH neurons, thus accelerating firing. The observed spontaneous KP release in MA mice also supports this view. The observed upregulation of receptors for neuropeptide FF, neuromedin U, melanocortin, natriuretic peptide, and parathyroid hormone suggests the involvement of additional neuropeptide signaling mechanisms.

Estradiol is an important regulator of GnRH neurons (Glanowska et al., 2012; Adams et al., 2018; Chen and Moenter, 2023). Both low (10 pM) and high (200 pM) doses of estradiol (Bálint et al., 2016; Farkas et al., 2018) decreased the firing activity of MA-GnRH neurons at diestrus, suggesting that the negative feedback of E2 remains functional during the early phase of reproductive senescence. Whether this effect is mediated directly or indirectly upon GnRH neurons requires further investigation.

In summary, we provided novel information about the changing transcriptome, cellular activity, and controlling mechanisms of GnRH neurons at middle age, the onset of reproductive senescence.

References

Adams C, Stroberg W, DeFazio RA, Schnell S, Moenter SM (2018) Gonadotropin-releasing hormone (GnRH) neuron excitability is regulated by estradiol feedback and kisspeptin. J Neurosci 38:1249–1263.

Agrawal A, et al. (2024) Wikipathways 2024: next generation pathway database. Nucleic Acids Res 52:D679–D689.

Bálint F, Liposits Z, Farkas I (2016) Estrogen receptor beta and 2-arachidonoylglycerol mediate the suppressive effects of estradiol on frequency of postsynaptic currents in gonadotropin-releasing hormone neurons of metestrous mice: an acute slice electrophysiological study. Front Cell Neurosci 10:77.

Balough JL, Dipali SS, Velez K, Kumar TR, Duncan FE (2024) Hallmarks of female reproductive aging in physiologic aging mice. Nat Aging 4:1711–1730.

Blighe K, Rana S, Lewis M (2024) EnhancedVolcano: publication-ready volcano plots with enhanced colouring and labeling. In. https://bioconductor.org/packages/EnhancedVolcano

Brinton RD, Yao J, Yin F, Mack WJ, Cadenas E (2015) Perimenopause as a neurological transition state. Nat Rev Endocrinol 11:393–405.

Burianova J, Ouda L, Profant O, Syka J (2009) Age-related changes in GAD levels in the central auditory system of the rat. Exp Gerontol 44:161–169.

Campbell RE, Han SK, Herbison AE (2005) Biocytin filling of adult gonadotropin-releasing hormone neurons in situ reveals extensive, spiny, dendritic processes. Endocrinology 146:1163–1169.

Campbell RE, Coolen LM, Hoffman GE, Hrabovszky E (2022) Highlights of neuroanatomical discoveries of the mammalian gonadotropin-releasing hormone system. J Neuroendocrinol 34:e13115.

Campos P, Herbison AE (2014) Optogenetic activation of GnRH neurons reveals minimal requirements for pulsatile luteinizing hormone secretion. Proc Natl Acad Sci U S A 111:18387–18392.

Caspary DM, Hughes LF, Ling LL (2013) Age-related GABAA receptor changes in rat auditory cortex. Neurobiol Aging 34:1486–1496.

Chang YM, Rosene DL, Killiany RJ, Mangiamele LA, Luebke JI (2005) Increased action potential firing rates of layer 2/3 pyramidal cells in the prefrontal cortex are significantly related to cognitive performance in aged monkeys. Cereb Cortex 15:409–418.

Chen X, Moenter SM (2023) Gonadal feedback alters the relationship between action potentials and hormone release in gonadotropin-releasing hormone neurons in male mice. J Neurosci 43:6717–6730.

Christian CA, Moenter SM (2008) Vasoactive intestinal polypeptide can excite gonadotropin-releasing hormone neurons in a manner dependent on estradiol and gated by time of day. Endocrinology 149:3130–3136.

Christian CA, Mobley JL, Moenter SM (2005) Diurnal and estradiol-dependent changes in gonadotropin-releasing hormone neuron firing activity. Proc Natl Acad Sci U S A 102:15682–15687.

Christian CA, Pielecka-Fortuna J, Moenter SM (2009) Estradiol suppresses glutamatergic transmission to gonadotropin-releasing hormone neurons in a model of negative feedback in mice. Biol Reprod 80:1128–1135.
Chu Z, Moenter SM (2005) Endogenous activation of metabotropic glutamate receptors modulates GABAergic transmission to gonadotropin-releasing hormone neurons and alters their firing rate: a possible local feedback circuit. J Neurosci 25:5740–5749.
Chu Z, Moenter SM (2006) Physiologic regulation of a tetrodotoxin-sensitive sodium influx that mediates a slow afterdepolarization potential in gonadotropin-releasing hormone neurons: possible implications for the central regulation of fertility. J Neurosci 26:11961–11973.
Chu Z, Tomaiuolo M, Bertram R, Moenter SM (2012) Two types of burst firing in gonadotrophin-releasing hormone neurones. J Neuroendocrinol 24:1065–1077.
Clarke H, Dhillo WS, Jayasena CN (2015) Comprehensive review on kisspeptin and its role in reproductive disorders. Endocrinol Metab (Seoul) 30:124–141.
Constantin S, Caraty A, Wray S, Duittoz AH (2009) Development of gonadotropin-releasing hormone-1 secretion in mouse nasal explants. Endocrinology 150:3221–3227.
Constantin S, Moenter SM, Piet R (2022) The electrophysiologic properties of gonadotropin-releasing hormone neurons. J Neuroendocrinol 34:e13073.
Czieselsky K, Prescott M, Porteous R, Campos P, Clarkson J, Steyn FJ, Campbell RE, Herbison AE (2016) Pulse and surge profiles of luteinizing hormone secretion in the mouse. Endocrinology 157:4794–4802.
DeFazio RA, Heger S, Ojeda SR, Moenter SM (2002) Activation of a-type gamma-aminobutyric acid receptors excites gonadotropin-releasing hormone neurons. Mol Endocrinol 16:2872–2891.
de Magalhães JP, Curado J, Church GM (2009) Meta-analysis of age-related gene expression profiles identifies common signatures of aging. Bioinformatics 25:875–881.
Farkas I, Vastagh C, Farkas E, Bálint F, Skrapits K, Hrabovszky E, Fekete C, Liposits Z (2016) Glucagon-like peptide-1 excites firing and increases GABAergic miniature postsynaptic currents (mPSCs) in gonadotropin-releasing hormone (GnRH) neurons of the male mice via activation of nitric oxide (NO) and suppression of endocannabinoid signaling pathways. Front Cell Neurosci 10:214.
Farkas I, Bálint F, Farkas E, Vastagh C, Fekete C, Liposits Z (2018) Estradiol increases glutamate and GABA neurotransmission into GnRH neurons via retrograde NO-signaling in proestrous mice during the positive estradiol feedback period. eNeuro 5:ENEURO.0057-18.2018.
Flurkey K, Currer JM, Harrison DE (2007) Mouse models in aging research. In: *The mouse in biomedical research*, Ed 2 (Fox JG, Davisson MT, Barthold SW, Newcomer CE, eds), pp 637–690. Amsterdam: Academic Press.
Frick KM, Burlingame LA, Arters JA, Berger-Sweeney J (2000) Reference memory, anxiety and estrous cyclicity in C57BL/6NIA mice are affected by age and sex. Neuroscience 95:293–307.
Furuya WI, Colombari E, Ferguson AV, Colombari DS (2017) Effects of acetylcholine and cholinergic antagonists on the activity of nucleus of the solitary tract neurons. Brain Res 1659:136–141.
Glanowska KM, Venton BJ, Moenter SM (2012) Fast scan cyclic voltammetry as a novel method for detection of real-time gonadotropin-releasing hormone release in mouse brain slices. J Neurosci 32:14664–14669.
Gold JR, Bajo VM (2014) Insult-induced adaptive plasticity of the auditory system. Front Neurosci 8:110.
Gore AC, Oung T, Yung S, Flagg RA, Woller MJ (2000) Neuroendocrine mechanisms for reproductive senescence in the female rat: gonadotropin-releasing hormone neurons. Endocrine 13:315–323.
Gore AC, Windsor-Engnell BM, Terasawa E (2004) Menopausal increases in pulsatile gonadotropin-releasing hormone release in a nonhuman primate (*Macaca mulatta*). Endocrinology 145:4653–4659.
Griffith WH, Dubois DW, Fincher A, Peebles KA, Bizon JL, Murchison D (2014) Characterization of age-related changes in synaptic transmission onto F344 rat basal forebrain cholinergic neurons using a reduced synaptic preparation. J Neurophysiol 111:273–286.
Gu Z, Eils R, Schlesner M (2016) Complex heatmaps reveal patterns and correlations in multidimensional genomic data. Bioinformatics 32:2847–2849.
Gustavsen JA, Pai S, Isserlin R, Demchak B, Pico AR (2019) RCy3: network biology using Cytoscape from within R. F1000Res 8:1774.
Gutiérrez A, Khan ZU, Ruano D, Miralles CP, Vitorica J, De Blas AL (1996) Aging-related subunit expression changes of the GABAA receptor in the rat hippocampus. Neuroscience 74:341–348.
Gutiérrez A, Khan ZU, Miralles CP, Mehta AK, Ruano D, Araujo F, Vitorica J, De Blas AL (1997) GABAA receptor subunit expression changes in the rat cerebellum and cerebral cortex during aging. Brain Res Mol Brain Res 45:59–70.
Han SK, Gottsch ML, Lee KJ, Popa SM, Smith JT, Jakawich SK, Clifton DK, Steiner RA, Herbison AE (2005) Activation of gonadotropin-releasing hormone neurons by kisspeptin as a neuroendocrine switch for the onset of puberty. J Neurosci 25:11349–11356.
Herbison AE, Moenter SM (2011) Depolarising and hyperpolarising actions of GABA(a) receptor activation on gonadotrophin-releasing hormone neurones: towards an emerging consensus. J Neuroendocrinol 23:557–569.
Hiraizumi Y, Nishimura I, Ishii H, Tanaka N, Takeshita T, Sakuma Y, Kato M (2008) Rat GnRH neurons exhibit large conductance voltage- and Ca2+-activated K+ (BK) currents and express BK channel mRNAs. J Physiol Sci 58:21–29.
Hoffman GE, Finch CE (1986) LHRH neurons in the female C57BL/6J mouse brain during reproductive aging: no loss up to middle age. Neurobiol Aging 7:45–48.
Hu L, Wada K, Mores N, Krsmanovic LZ, Catt KJ (2006) Essential role of G protein-gated inwardly rectifying potassium channels in gonadotropin-induced regulation of GnRH neuronal firing and pulsatile neurosecretion. J Biol Chem 281:25231–25240.
Imamov O, Shim GJ, Warner M, Gustafsson JA (2005) Estrogen receptor beta in health and disease. Biol Reprod 73:866–871.
Iremonger KJ, Constantin S, Liu X, Herbison AE (2010) Glutamate regulation of GnRH neuron excitability. Brain Res 1364:35–43.
Irizarry RA, Hobbs B, Collin F, Beazer-Barclay YD, Antonellis KJ, Scherf U, Speed TP (2003) Exploration, normalization, and summaries of high density oligonucleotide array probe level data. Biostatistics 4:249–264.
Jaffe DB, Brenner R (2018) A computational model for how the fast afterhyperpolarization paradoxically increases gain in regularly firing neurons. J Neurophysiol 119:1506–1520.
Kalló I, Vida B, Deli L, Molnár CS, Hrabovszky E, Caraty A, Ciofi P, Coen CW, Liposits Z (2012) Co-localisation of kisspeptin with galanin or neurokinin B in afferents to mouse GnRH neurones. J Neuroendocrinol 24:464–476.
Kauffman AS (2022) Neuroendocrine mechanisms underlying estrogen positive feedback and the LH surge. Front Neurosci 16:953252.
Kauffmann A, Gentleman R, Huber W (2009) Arrayqualitymetrics–a bioconductor package for quality assessment of microarray data. Bioinformatics 25:415–416.
Kermath BA, Gore AC (2012) Neuroendocrine control of the transition to reproductive senescence: lessons learned from the female rodent model. Neuroendocrinology 96:1–12.
Khodosevich K, Inta D, Seeburg PH, Monyer H (2007) Gene expression analysis of in vivo fluorescent cells. PLoS One 2:e1151.
Klaus B, Reisenauer S (2016) An end to end workflow for differential gene expression using Affymetrix microarrays. F1000Res 5:1384.
Knobil E (1988) The neuroendocrine control of ovulation. Hum Reprod 3:469–472.
Korach KS (1994) Insights from the study of animals lacking functional estrogen receptor. Science 266:1524–1527.
Kuehl-Kovarik MC, Pouliot WA, Halterman GL, Handa RJ, Dudek FE, Partin KM (2002) Episodic bursting activity and response to excitatory amino acids in acutely dissociated gonadotropin-releasing hormone neurons genetically targeted with green fluorescent protein. J Neurosci 22:2313–2322.
León S, et al. (2016) Direct actions of kisspeptins on GnRH neurons permit attainment of fertility but are insufficient to fully preserve gonadotropic axis activity. Sci Rep 6:19206.
Ling LL, Hughes LF, Caspary DM (2005) Age-related loss of the GABA synthetic enzyme glutamic acid decarboxylase in rat primary auditory cortex. Neuroscience 132:1103–1113.
Liposits Z, Sétáló G, Flerkó B (1984) Application of the silver-gold intensified 3,3′-diaminobenzidine chromogen to the light and electron microscopic detection of the luteinizing hormone-releasing hormone system of the rat brain. Neuroscience 13:513–525.
Liu X, Herbison AE (2008) Small-conductance calcium-activated potassium channels control excitability and firing dynamics in gonadotropin-releasing hormone (GnRH) neurons. Endocrinology 149:3598–3604.
Liu X, Herbison AE (2013) Dopamine regulation of gonadotropin-releasing hormone neuron excitability in male and female mice. Endocrinology 154:340–350.

Liu X, Herbison AE (2014) RF9 excitation of GnRH neurons is dependent upon Kiss1r in the adult male and female mouse. Endocrinology 155: 4915–4924.

Luebke JI, Chang YM, Moore TL, Rosene DL (2004) Normal aging results in decreased synaptic excitation and increased synaptic inhibition of layer 2/3 pyramidal cells in the monkey prefrontal cortex. Neuroscience 125:277–288.

Matsuo H, Baba Y, Nair RM, Arimura A, Schally AV (1971) Structure of the porcine LH- and FSH-releasing hormone. I. The proposed amino acid sequence. Biochem Biophys Res Commun 43:1334–1339.

Matt DW, Gilson MP, Sales TE, Krieg RJ, Kerbeshian MC, Veldhuis JD, Evans WS (1998) Characterization of attenuated proestrous luteinizing hormone surges in middle-aged rats by deconvolution analysis. Biol Reprod 59:1477–1482.

Merchenthaler I, Kovacs G, Lavasz G, Setalo G (1980) The preoptico-infundibular LH-RH tract of the rat. Brain Res 198:63–74.

Moenter SM, Chu Z, Christian CA (2009) Neurobiological mechanisms underlying oestradiol negative and positive feedback regulation of gonadotrophin-releasing hormone neurones. J Neuroendocrinol 21:327–333.

Moenter SM, Silveira MA, Wang L, Adams C (2020) Central aspects of systemic oestradiol negative- and positive-feedback on the reproductive neuroendocrine system. J Neuroendocrinol 32:e12724.

Nelson JF, Felicio LS, Osterburg HH, Finch CE (1981) Altered profiles of estradiol and progesterone associated with prolonged estrous cycles and persistent vaginal cornification in aging C57BL/6J mice. Biol Reprod 24: 784–794.

Nelson JF, Felicio LS, Randall PK, Sims C, Finch CE (1982) A longitudinal study of estrous cyclicity in aging C57BL/6J mice: I. Cycle frequency, length and vaginal cytology. Biol Reprod 27:327–339.

Nelson JF, Felicio LS, Osterburg HH, Finch CE (1992) Differential contributions of ovarian and extraovarian factors to age-related reductions in plasma estradiol and progesterone during the estrous cycle of C57BL/6J mice. Endocrinology 130:805–810. . doi:.

Norberg R, Campbell R, Suter KJ (2013) Ion channels and information processing in GnRH neuron dendrites. Channels (Austin) 7:135–145.

Oakley AE, Clifton DK, Steiner RA (2009) Kisspeptin signaling in the brain. Endocr Rev 30:713–743.

Parkening TA, Collins TJ, Smith ER (1982) Plasma and pituitary concentrations of LH, FSH, and prolactin in aging C57BL/6 mice at various times of the estrous cycle. Neurobiol Aging 3:31–35.

Parry BL (2008) Perimenopausal depression. Am J Psychiatry 165:23–27.

Pielecka-Fortuna J, Chu Z, Moenter SM (2008) Kisspeptin acts directly and indirectly to increase gonadotropin-releasing hormone neuron activity and its effects are modulated by estradiol. Endocrinology 149:1979–1986.

Piet R, Herbison AE (2018) Electrophysiology of rodent GnRH neurons. In: *The GnRH neuron and its control* (Herbison AE, Plant TM, eds), pp 177–202. UK: John Wiley and Sons Ltd.

Pitteloud N, et al. (2006) Mutations in fibroblast growth factor receptor 1 cause both kallmann syndrome and normosmic idiopathic hypogonadotropic hypogonadism. Proc Natl Acad Sci U S A 103:6281–6286.

Pitteloud N, et al. (2007) Loss-of-function mutation in the prokineticin 2 gene causes Kallmann syndrome and normosmic idiopathic hypogonadotropic hypogonadism. Proc Natl Acad Sci U S A 104:17447–17452.

Randall AD, Booth C, Brown JT (2012) Age-related changes to Na+ channel gating contribute to modified intrinsic neuronal excitability. Neurobiol Aging 33:2715–2720.

Ritchie ME, Phipson B, Wu D, Hu Y, Law CW, Shi W, Smyth GK (2015) Limma powers differential expression analyses for RNA-sequencing and microarray studies. Nucleic Acids Res 43:e47.

Rizzo V, Richman J, Puthanveettil SV (2014) Dissecting mechanisms of brain aging by studying the intrinsic excitability of neurons. Front Aging Neurosci 6:337.

Roland AV, Moenter SM (2011) Glucosensing by GnRH neurons: inhibition by androgens and involvement of AMP-activated protein kinase. Mol Endocrinol 25:847–858.

Rønnekleiv OK, Bosch MA, Zhang C (2012) 17β-Oestradiol regulation of gonadotrophin-releasing hormone neuronal excitability. J Neuroendocrinol 24:122–130.

Rønnekleiv OK, Zhang C, Bosch MA, Kelly MJ (2015) Kisspeptin and gonadotropin-releasing hormone neuronal excitability: molecular mechanisms driven by 17β-estradiol. Neuroendocrinology 102:184–193.

Rozycka A, Liguz-Lecznar M (2017) The space where aging acts: focus on the GABAergic synapse. Aging Cell 16:634–643.

Rubin BS, Lee CE, King JC (1994) A reduced proportion of luteinizing hormone (LH)-releasing hormone neurons express Fos protein during the preovulatory or steroid-induced LH surge in middle-aged rats. Biol Reprod 51:1264–1272.

Santoro N, Roeca C, Peters BA, Neal-Perry G (2021) The menopause transition: signs, symptoms, and management options. J Clin Endocrinol Metab 106:1–15.

Scarbrough K, Wise PM (1990) Age-related changes in pulsatile luteinizing hormone release precede the transition to estrous acyclicity and depend upon estrous cycle history. Endocrinology 126:884–890.

Shannon P, Markiel A, Ozier O, Baliga NS, Wang JT, Ramage D, Amin N, Schwikowski B, Ideker T (2003) Cytoscape: a software environment for integrated models of biomolecular interaction networks. Genome Res 13:2498–2504.

Shostak MD, Constantin S, Flannery J, Wray S (2023) Acetylcholine regulation of GnRH neuronal activity: a circuit in the medial septum. Front Endocrinol (Lausanne) 14:1147554.

Silverman AJ, Krey LC, Zimmerman EA (1979) A comparative study of the luteinizing hormone releasing hormone (LHRH) neuronal networks in mammals. Biol Reprod 20:98–110.

Spergel DJ (2019) Neuropeptidergic modulation of GnRH neuronal activity and GnRH secretion controlling reproduction: insights from recent mouse studies. Cell Tissue Res 375:179–191.

Spergel DJ, Catt KJ, Rojas E (1996) Immortalized GnRH neurons express large-conductance calcium-activated potassium channels. Neuroendocrinology 63:101–111.

Spergel DJ, Krüth U, Hanley DF, Sprengel R, Seeburg PH (1999) GABA- and glutamate-activated channels in green fluorescent protein-tagged gonadotropin-releasing hormone neurons in transgenic mice. J Neurosci 19:2037–2050.

Subramanian A, et al. (2005) Gene set enrichment analysis: a knowledge-based approach for interpreting genome-wide expression profiles. Proc Natl Acad Sci U S A 102:15545–15550.

Sung KW, Kirby M, McDonald MP, Lovinger DM, Delpire E (2000) Abnormal GABAA receptor-mediated currents in dorsal root ganglion neurons isolated from Na-K-2Cl cotransporter null mice. J Neurosci 20: 7531–7538.

Suter KJ, Wuarin JP, Smith BN, Dudek FE, Moenter SM (2000) Whole-cell recordings from preoptic/hypothalamic slices reveal burst firing in gonadotropin-releasing hormone neurons identified with green fluorescent protein in transgenic mice. Endocrinology 141:3731–3736.

Todman MG, Han SK, Herbison AE (2005) Profiling neurotransmitter receptor expression in mouse gonadotropin-releasing hormone neurons using green fluorescent protein-promoter transgenics and microarrays. Neuroscience 132:703–712.

Vastagh C, Rodolosse A, Solymosi N, Farkas I, Auer H, Sárvári M, Liposits Z (2015) Differential gene expression in gonadotropin-releasing hormone neurons of male and metestrous female mice. Neuroendocrinology 102: 44–59.

Vastagh C, Farkas I, Csillag V, Watanabe M, Kalló I, Liposits Z (2024) Cholinergic control of GnRH neuron physiology and luteinizing hormone secretion in male mice: involvement of ACh/GABA cotransmission. J Neurosci 44:e1780232024.

Wang L, DeFazio RA, Moenter SM (2016) Excitability and burst generation of AVPV kisspeptin neurons are regulated by the estrous cycle via multiple conductances modulated by estradiol action. eNeuro 3: ENEURO.0094-16.2016.

Wang Y, Garro M, Dantzler HA, Taylor JA, Kline DD, Kuehl-Kovarik MC (2008) Age affects spontaneous activity and depolarizing afterpotentials in isolated gonadotropin-releasing hormone neurons. Endocrinology 149:4938–4947.

Wang Z, Wu W, Kim MS, Cai D (2021) GnRH pulse frequency and irregularity play a role in male aging. Nat Aging 1:904–918.

Watanabe M, Sakuma Y, Kato M (2009) GABAA receptors mediate excitation in adult rat GnRH neurons. Biol Reprod 81:327–332.

Wetsel WC, Valença MM, Merchenthaler I, Liposits Z, López FJ, Weiner RI, Mellon PL, Negro-Vilar A (1992) Intrinsic pulsatile secretory activity of immortalized luteinizing hormone-releasing hormone-secreting neurons. Proc Natl Acad Sci U S A 89:4149–4153.

Wise PM, Dueker E, Wuttke W (1988) Age-related alterations in pulsatile luteinizing hormone release: effects of long-term ovariectomy, repeated pregnancies and naloxone. Biol Reprod 39:1060–1066.

Womack MD, Hoang C, Khodakhah K (2009) Large conductance calcium-activated potassium channels affect both spontaneous firing and intracellular calcium concentration in cerebellar Purkinje neurons. Neuroscience 162:989–1000.

Wong TP, Marchese G, Casu MA, Ribeiro-da-Silva A, Cuello AC, De Koninck Y (2000) Loss of presynaptic and postsynaptic structures is accompanied by compensatory increase in action potential-dependent synaptic input to layer V neocortical pyramidal neurons in aged rats. J Neurosci 20:8596–8606.

Wray S, Grant P, Gainer H (1989) Evidence that cells expressing luteinizing hormone-releasing hormone mRNA in the mouse are derived from progenitor cells in the olfactory placode. Proc Natl Acad Sci U S A 86:8132–8136.

Xie Q, Kang Y, Zhang C, Xie Y, Wang C, Liu J, Yu C, Zhao H, Huang D (2022) The role of kisspeptin in the control of the hypothalamic-pituitary-gonadal axis and reproduction. Front Endocrinol (Lausanne) 13:925206.

Xu C, Xu XZ, Nunemaker CS, Moenter SM (2004) Dose-dependent switch in response of gonadotropin-releasing hormone (GnRH) neurons to GnRH mediated through the type I GnRH receptor. Endocrinology 145:728–735.

Xu S, et al. (2024) Using clusterProfiler to characterize multiomics data. Nat Protoc 19:3292–3320.

Yamamoto R, Chung R, Vazquez JM, Sheng H, Steinberg PL, Ioannidis NM, Sudmant PH (2022) Tissue-specific impacts of aging and genetics on gene expression patterns in humans. Nat Commun 13:5803.

Yan J, Zhang Y, Roder J, McDonald RJ (2003) Aging effects on spatial tuning of hippocampal place cells in mice. Exp Brain Res 150:184–193.

Yan Y, Cheng L, Chen X, Wang Q, Duan M, Ma J, Zhao L, Jiang X, Ai J (2017) Estrogen deficiency is associated with hippocampal morphological remodeling of early postmenopausal mice. Oncotarget 8:21892–21902.

Yokoyama T, Minami K, Terawaki K, Miyano K, Ogata J, Maruyama T, Takeuchi M, Uezono Y, Ueta Y (2014) Kisspeptin-10 potentiates miniature excitatory postsynaptic currents in the rat supraoptic nucleus. Brain Res 1583:45–54.

Yu ZY, Wang W, Fritschy JM, Witte OW, Redecker C (2006) Changes in neocortical and hippocampal GABAA receptor subunit distribution during brain maturation and aging. Brain Res 1099:73–81.

Zhang C, Roepke TA, Kelly MJ, Rønnekleiv OK (2008) Kisspeptin depolarizes gonadotropin-releasing hormone neurons through activation of TRPC-like cationic channels. J Neurosci 28:4423–4434.